REPORT SERIES IN AEROSOL SCIENCE
N:o 162 (2015)

FINE PARTICLE FORMATION IN BIOMASS COMBUSTION AND FLAME SYNTHESIS – MORPHOLOGICAL FEATURES AND TOXICITY

TIINA TORVELA

Faculty of Science and Forestry
University of Eastern Finland
Kuopio, Finland

Academic dissertation
To be presented, with the permission of the Faculty of Science and Forestry of the University of Eastern Finland, for public examination in auditorium SN201, Snellmania Building, at the University of Eastern Finland, Kuopio, on February 27 2015, at 12 o'clock noon.

Kuopio 2015

Author's address:
Fine particle and Aerosol Technology Laboratory
University of Eastern Finland
Department of Environmental Science
P.O.Box 1627
70211 KUOPIO
FINLAND
email: tiina.torvela@uef.fi

Supervisors:
Professor Jorma Jokiniemi, Ph.D.
University of Eastern Finland
Department of Environmental Sciences

Doctor Jarkko Tissari, Ph.D.
University of Eastern Finland
Department of Environmental Sciences

Doctor Anna Lähde, Ph.D.
University of Eastern Finland
Department of Environmental Sciences

Reviewers:
Professor Jyrki Mäkelä, Ph.D.
Tampere University of Technology
Department of Physics
Tampere, Finland

Research Professor Hannu Norppa, Ph.D.
Finnish Institute of Occupational Health
Health and Work Ability
Helsinki, Finland

Opponent:
Associate Professor Joakim Pagels, Ph.D.
Lund University
Department of Design Sciences
Lund, Sweden

ISBN 978-952-7091-12-8 (printed version)
ISSN 0784-3496
Helsinki 2015
Unigrafia Oy

ISBN 978-952-7091-13-5 (pdf version)
http://www.atm.helsinki.fi/FAAR/
Helsinki 2015

Tiina Maria Torvela
University of Eastern Finland, 2015

ABSTRACT

In this thesis, the fine particle formation process in flames is assessed according to morphological features, such as size, shape, solid phase, and texture. These relationships are of significant importance when particle-induced effects on atmospheric environment and human health are to be evaluated. Moreover, the role of zinc and its physical and chemical properties on the particle-induced toxic response *in vitro* was studied.

First, a theoretical background of the processes affecting particle formation in the gas phase is briefly introduced. The conditions that affect particle formation in biomass combustion processes are then discussed. Second, the field of nanomaterial engineering is introduced. Third, the complex roles of zinc in the particle-mediated toxicity observed in epidemiological studies in humans, *in vitro* and *in vivo* are discussed.

In the experimental part of this thesis, biomass combustion derived particulate mass was generated via the controlled combustion of wood chips and by varying the efficiency of the combustion. Additionally, a series of woody pellets with different amounts of added zinc were burned to study the zinc fractionation into ultrafine particulate mass. Then, ultrafine particles with compositional similarity to the combustion-generated ash were manufactured via flame combustion from liquid precursors. The conditions during the experiments were characterised using validated on-line and off-line aerosol methods. The particles with aerodynamic sizes below one micrometre were collected and thoroughly characterised, and their toxicological properties were tested using a mouse macrophage cell model.

New information was obtained about the heterogeneous speciation of materials in combustion-generated particulate mass and the solid material characteristics of particulate mass produced from zinc-enriched biomass. These issues were studied using methods from materials science and aerosol technology. Moreover, the toxicological analyses were of significant importance to demonstrate which properties of particles should be considered toxicologically relevant. The study revealed that the heterogeneous nature of emission is poorly defined by the average bulk values. Moreover, the morphological properties of biomass fuel are directly related the toxicity of the emissions.

Keywords: aerosols, biomass, combustion, electron microscopy, emissions, fine particles, toxicity

Acknowledgements

This research was made possible by a co-operation of the Inhalation toxicology and the Fine particle and aerosol technology laboratories of the University of Eastern Finland. I wish to express my gratitude to both group leaders, Prof. Maija-Riitta Hirvonen and Prof. Jorma Jokiniemi, for a great scientific environment for such work.

I am grateful to my principal supervisor Prof. Jorma Jokiniemi for guidance and inspiring assignments at FINE. I am deeply thankful to my supervisor PhD Jarkko Tissari for enlightening conversations and sharing his knowledge on combustion. I am equally thankful for my supervisor PhD, Doc Anna Lähde for sharing her expertise, and for her enthusiasm towards my work. I am also grateful to PhD, Doc Jorma Joutsensaari for improving my thesis, and for his support at every stage of my work.

I am grateful to the examiners of the thesis, Prof. Jyrki Mäkelä and Res. Prof. Hannu Norppa, for their valuable comments. I wish to thank Assoc. Prof. Joakim Pagels for kindly accepting the invitation to serve as an opponent in the public examination of my thesis.

I dedicate my warmest thanks to all of the researchers involved in the experimental part of this thesis, especially PhD Oskari Uski, MSc Tommi Karhunen and PhD Olli Sippula. I also wish to thank Sib-Labs team for their valuable help. I thank my present and past team members for help and sharing ideas.

Financial support from the Academy of Finland, Finnish Funding Agency for Technology and Innovation, and University of Eastern Finland are acknowledged with gratitude.

Finally, I wish to thank my parents and friends for support and times spend with sports and music. My husband Pekka I thank for endless amount of inspiration, respect and love during the years.

Kuopio Jan 29, 2015 *Tiina Torvela*

Abbreviations

BF	Bright field
C_{MFZ}	Maximum free zinc ion concentration
CPC	Condensation particle counter
DF	Dark field
DGI	Dekati gravimetric impactor
DLPI	Dekati low-pressure impactor
DMA	Differential mobility analyzer
DMSO	Dimethyl sulfoxide C_2H_6OS
DP	Diffraction pattern
EC	Elemental carbon
ED	Ejector diluter
EDS	Energy dispersive X-ray spectrometry
ELPI	Electrical low-pressure impactor
FMPS	Fast mobility particle sizer
FSP	Flame spray pyrolysis
FTIR	Fourier transform infrared analyzer
IC	Ion chromatography
ICP-MS	Inductively coupled plasma mass spectrometer
MFC	Mass flow controller
MIP-2	Macrophage inflammatory protein 2
OC	Organic carbon
OGC	Organic gaseous compounds
OTM	Olive tail moment
PAH	Polycyclic aromatic hydrocarbons
PI	Propidium iodide
PIXE	Proton induced X-ray emission
PM_i	Mass of particles below aerodynamic diameter of i μm
PRD	Porous tube diluter
PTFE	Polytetrafluoroethylene
ROS	Reactive oxygen species
SAED	Selected area electron diffraction
SCGE	Single cell gel electrophoresis
SMPS	Scanning mobility particle sizer
TEM	Transmission electron microscopy
TEOM	Tapered element oscillating microbalance
TNF-α	Tumor necrosis factor alpha
UFP	Ultrafine particles
XRD	X-ray diffractometry

LIST OF PUBLICATIONS

This thesis consists of the present review of the author's work in the field of aerosol and materials science and the following selection of the author's publications:

I T. Torvela, J. Tissari, O. Sippula, T. Kaivosoja, J. Leskinen, A. Virén, A. Lähde, and J. Jokiniemi , "Effect of wood combustion conditions on the morphology of freshly emitted fine particles," *Atmos. Environ.* **87,** 65–76 (2014).

II T. Torvela, O. Uski, T. Karhunen, O. Sippula, P. Jalava, M-R. Hirvonen, J. Jokiniemi, and A. Lähde, "Reference particles for toxicological studies of wood combustion: formation, characteristics and toxicity compared to those of real wood combustion particulate mass," *Chem. Res. Toxicol.* **27,** 1516–1527 (2014).

III J. Tissari, O. Sippula, T. Torvela, H. Lamberg, J. Leskinen, S. Paukkunen, M.-R. Hirvonen, J. Jokiniemi, "Zinc nanoparticle formation and physicochemical properties in wood combustion - experiments with Zn-doped pellets in a small-scale boiler," *Fuel* **143,** 404–413 (2015).

IV O. Uski, P.I Jalava, M.S Happo, T. Torvela, J. Leskinen, J. Mäki-Paakkanen; J. Tissari, O. Sippula, H. Lamberg, J. Jokiniemi, M.-R. Hirvonen, "Effect of fuel zinc content on toxicological responses of particulate matter from pellet combustion *in vitro*," *Sci. Total Environ.* **511,** 331–340 (2015).

Throughout the overview, these papers will be referred to by Roman numerals. Publications **II** and **IV** were previoysly included in a doctoral thesis by Oskari Uski [1]. The thesis of Uski concentrated on the toxic effects of the emissions, while the ojectives of this thesis are the formation, composition and morphology of the emissions.

Contents

1 INTRODUCTION **9**

1.1 Background and motivation 9
1.2 Objectives of the study 11

2 SCIENTIFIC BACKGROUND **13**

2.1 Aerosols in the environment 13
2.2 Formation and growth of aerosol particles 13
2.3 Particles from combustion processes 15
2.3.1 Flame types 15
2.3.2 Biomass fuel and combustion emissions . . . 16
2.3.3 Soot particles 17
2.3.4 Particulate organic matter 19
2.3.5 Ash species 19
2.4 Nanomaterials 21
2.4.1 Nanomaterial properties 21
2.4.2 Manufacture and engineering of nanomaterials 22
2.5 Solid state properties of nanomaterials and zinc oxide 23
2.5.1 Crystalline, polycrystalline, nanocrystalline, amorphous 23
2.5.2 Zinc oxide 24
2.6 Health effects of particle exposure 25
2.6.1 Adverse health effects via a pulmonary route 25
2.6.2 Mechanisms of particle induced toxicity . . . 26
2.6.3 Toxicity of zinc 27
2.7 The importance of studying morphology 28

3 EXPERIMENTAL METHODS **31**

3.1 Biomass combustion appliances 31
3.2 Flame spray synthesis 33
3.3 Measurements and materials analyses 34
3.3.1 Particle number and mass size distributions . 34

3.3.2 Chemical analyses 35
3.3.3 Gas emission analyses 35
3.3.4 X-ray diffractometry 36
3.3.5 Transmission electron microscopy (TEM) . . . 37
3.4 Calculations 38
3.4.1 Real-time gas and particle concentration data 38
3.4.2 Thermodynamic equilibrium calculations . . . 39
3.5 Study design for toxicological studies 40

4 RESULTS AND DISCUSSION 43
4.1 Review of papers 43
4.2 Particle formation in biomass combustion in variable conditions 44
4.2.1 Mixing state of the particles 45
4.2.2 Soot structure 47
4.2.3 Inorganic particles 49
4.3 Particle formation in biomass combustion with varying zinc concentrations 54
4.4 Formation of engineered nanoparticles 57
4.5 Toxic effects of the particles 58

5 AUTHOR'S CONTRIBUTION 65

6 CONCLUSIONS 67

BIBLIOGRAPHY 70

1 Introduction

1.1 BACKGROUND AND MOTIVATION

Inhaled air consists of various gases, liquids and solid particulate matter (PM). The properties (e.g., composition and concentration) of the PM affect the atmosphere and human health locally, globally and at every scale in between. It has been estimated that anthropogenic $PM_{2.5}$ (PM with and aerodynamic diameter below 2.5 μm) causes 2.1 million premature deaths each year due to cardiopulmonary diseases and lung cancer [2]. Small-scale biomass combustion is responsible for a substantial portion of the total PM emissions [3]. These emissions are likely to increase substantially due to the decision by the EU to increase the use of renewable energy to up to 20 % of the total energy consumption [4].

At the same time, increasing amounts of nanomaterials are produced [5]. The effects of the increasing use of these materials has not yet been evaluated epidemiologically, but the accumulating evidence for the increased toxicity of pure nanomaterials has raised a discussion about whether restrictions should be implemented for the production and use of these materials [5]. Zinc oxide (ZnO) nanomaterials are produced and used in many commercial applications, such as sunscreens and antibacterial coatings [6]. Zinc is an essential trace metal for animal and plant cells that takes part in many cell metabolic functions [7]. Excess ionic zinc is known to induce cascading inflammatory reactions in cells, eventually leading to cell apoptosis and necrosis [7].

Previously, many epidemiological studies that have been conducted on $PM_{2.5}$ or PM_{10} accentuate the role of the carbonaceous contents of the PM [8]. The ultrafine PM fraction was thought to play a minor role in particle-induced human health effects because of its low mass fraction in PM. However, research on engineered nanomaterials has identified connections between nanoparticle toxicity and individual particle properties, such as a high surface-to-

mass ratio [9]. Interest in metrics other than mass to describe particle toxicity has gained traction [10].

Moreover, recent studies have shown that the carbonaceous content of ultrafine PM does not fully describe its toxicological properties, especially in near complete combustion where the fraction of carbonaceous species is usually low [11, 12]. The possibility of metal oxide accumulation in PM in high temperature combustion was recognised in coal combustion studies in the 1980s [13]. A possible role for ZnO and other transition metal oxides in the toxicity of PM has been hypothesised since [14, 15].

The formation of ZnO in synthetic processes has been intensively studied and is well known, especially electrodeposition on surfaces [6]. However, there is little information on the formation and fractionation of ZnO and zinc containing species in biomass combustion, especially in the inhalable particle fraction. In particular, the morphological features, e.g., the size, shape, and phase, of the zinc in ultrafine particulate emission are largely unknown. Electron microscopy studies assessing those properties are uncommon, especially for fresh emissions from biomass combustion [16].

In this study, knowledge of ZnO binding in biomaterials and synthetic nanomaterials is complemented with new research findings which show that ZnO accumulates in the ultrafine particulate emission from biomass combustion. The characteristics of the biomass PM are compared with those of engineered nanoparticles, and the possible role of the observed features in the toxicity of both is discussed. The formation of zinc containing particles is discussed with a focus on the morphology of ultrafine particles resulting from the biomass combustion. The study provides new information about how the zinc in biomass fuels contributes to ultrafine PM emission.

1.2 OBJECTIVES OF THE STUDY

This study focuses on the morphological features and physico-chemical properties of (a) particle emissions originating from biomass combustion and (b) flame engineered nanoparticles, with the following detailed objectives :

1. To understand the effects of the combustion conditions on the formation of fine particulate mass (Papers **I**-**III**);

2. To understand the connection between the chemical speciation in biomass combustion and the particle morphology (Paper **I**);

3. To determine the key physical and chemical features of ultrafine ash particles that are responsible for their toxicity (Paper **II**);

4. To understand the behaviour of zinc in efficient wood combustion processes (Paper **III**), and the role of zinc in the toxicity of these emissions (Papers **II**-**IV**)

2 Scientific background

2.1 AEROSOLS IN THE ENVIRONMENT

Aerosols are mixtures of liquid or solid particles suspended in a gas. Atmospheric PM is commonly divided into ultrafine, fine, and coarse particle size fractions, which refer to particles with aerodynamic diameters smaller than 0.1 μm ($PM_{0.1}$) or 2.5 μm ($PM_{2.5}$) or in the range of 2.5–10 μm ($PM_{2.5}$-PM_{10}), respectively [17]. Ultrafine particles can also be classified as *nanoparticles* in materials sciences.

Aerosols play important roles in atmospheric processes, including both global climate and local air quality. Aerosols contribute to the radiation balance on the Earth by scattering solar radiation and taking part in cloud formation [18]. Aerosols are naturally formed in biogenic, geogenic and oceanogenic processes, as well as from the burning of meteoroids as they fall [19]. Man-made, that is anthropogenic, atmospheric particles are emissions from industrial operations, farming, and combustion processes.

Multiple epidemiological studies provide compelling evidence that PM contributes more to the adverse health effects observed in humans than pollution gases (e.g. ozone, CO and nitrogen gases) [20]. In particular, particle emissions from residential wood combustion, coal and oil combustion, traffic, and the metal industry can be considered sources with extensive health risks [21, 22].

2.2 FORMATION AND GROWTH OF AEROSOL PARTICLES

The formation and growth of new aerosol particles changes both the size and composition distributions of the aerosol. This dynamic process, called gas-to-particle conversion [23], is affected by the chemical reaction rates in the system and can be described by various subprocesses [24]: i) reactions of gas molecules, ii) nucleation of vapours, iii) vapour condensation onto the surfaces of pre-existing

particles, iv) reactions on the surfaces of existing particles, and v) reactions and/or ordering of molecules within particles. In addition, coagulation (agglomeration) occur at any stage because of the high number concentration of the primary particles. Each of these steps can also be observed as rate-determining processes in particle formation and growth [23]; for example, the chemical reaction rate of SO_2 to SO_3 may slow down the formation of K_2SO_4 in the gas phase [25].

In the gas, molecules collide at high speeds. The collision rate is described using the mean free path, and it is determined by the gas state (temperature, pressure, and volume) [19]. The collision of molecules may lead to chemical reactions (i). The reactions are in equilibrium when the system has the lowest Gibbs free energy [26].

Some of the reactions, e.g., the oxidation of metals, lead to the formation of low vapour pressure species, which may change phase to minimise the energy [27]. Nucleation (ii) is a gas-to-particle conversion process, where particles are formed directly from the gas phase [19]. The driving force in the nucleation process is the change in the system free energy, either due to the change in the surrounding gas state (e.g., volume, temperature, and pressure), or due to reactions (i). The gas is supersaturated when the partial pressure of a species is higher than the equilibrium vapour pressure of the gas for that species, at that temperature [23]. In high temperature reactions, such as flame combustion, supersaturation conditions usually occur when the combustion gases cool or when chemical reactions yield species with very low saturation vapour pressures [28].

Catalytic reactions and surface reactions (iv) may lead to alterations in the particle and gas composition [29]. The reaction rates at a particle surface are mechanistically described by the interaction between the particle and the gas molecules [19]. When catalysts, such as free radicals, are involved in the reaction, various chemical reaction rates may be increased.

Moreover, volume reactions (v) may result in significant changes in the particle chemistry and structure [23]. Sulfidation of metal and metal oxide nanoparticles, which starts as a surface reaction

and radially develops over the particle, is that type of reaction [30]. Many chemical reactions produce amorphous solids that change their phase via molecular ordering (i.e., crystal formation) in a volume reaction [30]. In general, these reactions are slower than gas phase processes.

Finally, the colliding primary particles may coagulate to reduce their surface free energy [19]. Larger spherical particles are formed if the colliding particles both aggregate and fuse (coalescence); agglomeration follows the high rate of collisions with a lesser extent of interparticle fusion [31]. In general, agglomerates are three-dimensional structures formed in an agglomeration process where physical or chemical bonding between the primary particles (sintering) occurs.

In an aerosol, the diffusive motion of the particles, known as Brownian motion or Brownian diffusion, result in particle – particle interactions and coagulation [23]. Compared with other transport mechanisms (thermal diffusion, thermophoresis, transport in an electrical field), Brownian diffusion is the most efficient one for nanoparticles [19, 32]. This also holds true for nanoparticle deposition in filter media. Moreover, in the lungs, Brownian diffusion is the dominant deposition mechanism during the pause between inhalation and exhalation [33].

2.3 PARTICLES FROM COMBUSTION PROCESSES

2.3.1 Flame types

In this study, two different types of flames, characterised by different mixing conditions of oxygen with fuel, were used to generate particles.

In a diffusion flame, combustion occurs at the flame surface where the fuel combines with the oxidant, e.g., hydroxide (OH), transported via diffusion [34]. A candle flame and pellet burner flame are examples of diffusion flames. In these flames, the chemical reaction rates are limited by the mass transport of the oxidant [34]. High soot production is typical of wood combustion in

diffusion flames [35]. In wood combustion appliances, more complete combustion can usually be achieved due to additional air staging to increase the mixing of oxygen with the flame, provided that the temperature is not significantly decreased [36].

In so-called pre-mixed flames, found for example in engines, the oxidant is mixed with the fuel before entering the flame [37]. Such mixing can produce multiple smaller flame fronts, where chemical reactions occur very fast as the oxidant does not need to be transported. In laboratory flame reactors, such as Flame Spray Pyrolysis (FSP), the pre-mixing of precursors with air or oxygen is utilised to create single metal oxides of high purity, such as TiO_2, Al_2O_3, PbO, Fe_2O_3, and ZnO, to name a few. In a pre-mixed flame FSP reactor, the typical flame temperatures are 2200-2600 K [37].

2.3.2 Biomass fuel and combustion emissions

In general, biomass is a material that has a biological origin. As a source of energy, biomass can be defined as wood, charcoal, agricultural residue or animal dung [22]. Globally, biomass is an important energy resource. There is growing interest in the use of biomass for the production of energy in the future [4]. Energy from biomass can be used for residential heating (e.g., wood stoves, boilers, and pellet burners) and industrial-scale power plants.

Biomass burning is considered the largest source of primary carbonaceous aerosol particles and a significant source of reactive trace gases into the Earth's atmosphere [21], as well as gas-phase nonmethane organic compounds [38]. It has been recently shown that biomass emissions may have a larger contribution on direct and indirect atmospheric radiative forcing than previously assumed [21].

The properties of biomass fuels, which make them different from fossil fuels, play important roles in aerosol formation during combustion. First, biomass fuels have high volatile material contents and low char contents compared with coal burning [39]. Thus, their heating values are lower than fossil fuels. Second, biomass ash contains high concentrations of alkali metal species, especially

potassium but also chlorine, sulphur and calcium. Third, the carbon is bound in cellulose, hemicellulose and lignin, which are thermally decomposed in pyrolysis to short-chained or ringed hydrocarbons [40].

In the complete combustion of hydrocarbons, only carbon dioxide (CO_2) and water (H_2O) are produced via the oxidation of the elemental carbon, hydrogen and oxygen in the fuel. Typical gaseous emissions also contain carbon monoxide (CO), sulphur dioxide (SO_2), nitrogen oxides (NO_x), oxygen (O_2) and hydrogen (H_2), as well as various gaseous hydrocarbons. In biomass combustion, the NO_x compounds are usually derived from the nitrogen in the fuel; however, at high flame temperatures, they can be formed via the thermal oxidation of the N_2 in air [41].

The particles released in combustion systems are usually classified as 1) soot, 2) inorganic particles, or 3) particulate organic matter [42]. Moreover, secondary reactions that produce liquid products, such as sulphuric acid (H_2SO_4), occur at exhaust temperatures. In the next sections, the main particulate aerosol types are briefly introduced.

2.3.3 Soot particles

In small-scale appliances, soot is a large fraction of the fine particle emissions due to non-optimal combustion conditions. The filtration technologies that are widely used in industrial scale appliances to reduce particle emission are not usually used in small-scale combustion.

From the chemical point of view, the soot is mostly composed of elemental carbon (EC) [35]. Soot particles are formed from gaseous hydrocarbons under fuel-rich, non-oxidising conditions inside (diffusion) flames [34]. The high collision rates of the hydrocarbons lead to the formation of larger groups and, finally, 1-2 nm nuclei, which grow further due to surface reactions and coagulation [43]. Polycyclic aromatic hydrocarbons (PAHs) play an important role in the formation of soot [40]. Soot is amorphous by default: finer

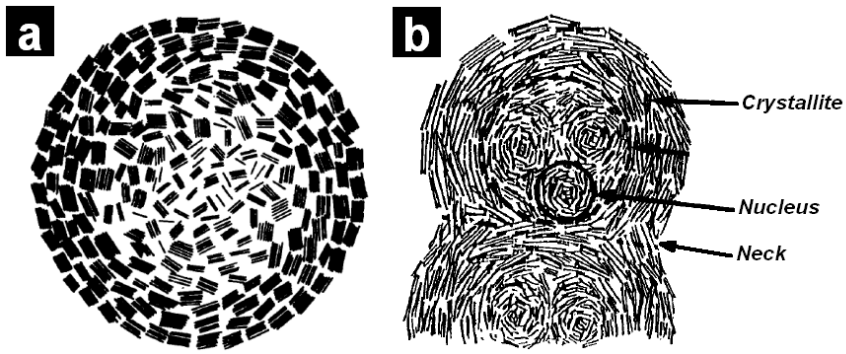

Figure 2.1: A schematic drawings on the nanostructure of (a) a single soot primary particle, showing crystallite ordering as concentric layers, and (b) part of a diesel soot agglomerate, showing crystallites ordered both as small nuclei and as outer shell forming layer. Also particle sintering, forming a neck between two primary particles in an agglomerate, is illustrated in (b). The image emphasizes the effect of formation condition on the structural refinement of soot: the diesel particles typically have more complicated fine structure than, for example, soot from wood combustion [46]. Adopted and modified from [47].

nanocrystalline structures can be formed at the end of the sooting via the carbonisation process [44]. Carbonisation requires a sufficient residence time at pyrolytic conditions to enable the conversion of an amorphous material into concentrically oriented, planar crystallites [43, 45] (Fig. 2.1).

Reactions with oxidants (OH, O and O_2) at high temperatures complete the primary soot and hydrocarbon combustion to the final gaseous products, CO and CO_2 [34]. However, in diffusion flames under fuel-rich conditions even with excess air, the combustion may be incomplete, and a large amount of soot particles and organic aerosols are emitted from the flame [34, 48].

The hot, small primary soot particles agglomerate rapidly to form branched structures [40]. Further surface reactions on soot agglomerates occur in the gas, whose equilibrium state is constantly changing due to changes in the temperature and gas volume due to dilution. Therefore, various species are condensed on the agglomerates [40]. Finally, the characteristics of the soot may change

significantly due atmospheric aging, for example, by reactions with atmospheric sulphuric acid [49].

2.3.4 Particulate organic matter

In parallel with soot, organic aerosols are derived from the fuel hydrocarbons and either transformed into CO and CO_2 in the combustion reaction or released from the flame into the exhaust gas due to incomplete combustion [48]. Moreover, reactions with atmospheric oxidants (OH, O_3 and NO_3) may create species that condense into the particulate phase [27] due to the lower vapour pressure of the new compounds.

Organic aerosols are also created in the atmosphere via secondary reactions [50]. Hundreds of compounds belong to this group. It has been estimated that at least 50-90 % of primary organic aerosol emissions consist of semivolatile organics, which are partially or completely in the vapour phase in ambient, diluted conditions [27]. This means that over the wide range of exhaust gas temperatures found in primary combustion sources, most of them are in the gaseous phase. In the aerosols produced from biomass combustion, the organic carbon content is relatively high when compared to those from fossil-fuel primary emissions [40].

A special group of organic aerosols are the PAHs. PAHs form through ring-coordinated polymerisation of hydrocarbons during the incomplete combustion of organic matter [43]. PAHs have received special attention due to their known toxicity and were one of the first atmospheric species identified as carcinogenic [23]. The volatilities of different PAHs range from highly volatile to completely condensed [51].

2.3.5 Ash species

Solid fuels always contain inorganic, refractory species. Some of the refractory components volatilise and form fine fly ash, whereas the involatile fraction remain either in the bottom ash or a small part may separate into the coarse fly ash fraction [52]. The temperature

is the main factor determining the release of ash, and the oxidation conditions affect the volatilisation because the reduced forms of many elements and ions are more volatile than their oxidised forms [27].

In wood combustion, the volatile alkali species, mostly potassium and sodium, react in the gas phase with available chlorine or sulphur [53], mainly forming sulphates (e.g. K_2SO_4, Na_2SO_4). Furthermore, alkali chlorides (KCl, NaCl) may be converted into sulphates if enough gaseous sulphur is present [54]. The release of alkali materials into the gas phase is strongest in the char combustion phase due to the reducing conditions near the burning particle surface [55].

High temperature processes also release trace metals, such as Fe, Zn, Cu, Cr, Co, and Pb, into the vapour phase. Metal particle formation in fly ash PM was first theoretically described in pulverised coal combustion [13]. In biomass combustion, the bed temperatures and fuel concentrations of the trace metals affect the release; thus, fewer heavy metals are released from biomass combustion than in coal combustion [56]. The trace metal speciation in different biofuel-combustion-derived PM has been reviewed by Sippula [57]. The chemical analyses show that Zn is the most abundant trace metal in biomass combustion PM.

There are a few studies that explain the Zn speciation in the biomass PM in more details [56, 58–61]; most of them are based on thermodynamic equilibrium calculations. Strand (2004) [58] suggested that the oxidising conditions in woody biofuel combustion lead to Zn enrichment in the fine PM as ZnO via a nucleation-condensation process, before the nucleation of K_2SO_4. Jöller *et al.* (2005, 2007) [56, 59] described the formation of heterogeneous fine ash structures containing separate ZnO and alkali salt particles but provided little speculation about waste wood combustion. Wiinikka *et al.* (2007) [60] and Sippula *et al.* (2009) [61] were the first to suggest ZnO formation as the first nucleation seeds for other condensing species in PM_1 from untreated wood combustion. All of these studies address the importance of the fuel ash composition on the

release and fractionation of Zn. That discussion is continued in Paper **III** and this thesis. Finally, direct evidence for ZnO in the PM samples had previously been provided from electron microscopy, but only on ambient (urban) samples, e.g., by Tumolva *et al.* [62]. To the best of our knowledge, Paper **I** and the current thesis are the first attempts to analyse the morphological features of ZnO nuclei in freshly emitted PM from untreated wood combustion.

2.4 NANOMATERIALS

2.4.1 Nanomaterial properties

Nanomaterials can be defined as materials that have one dimension between 1 and 100 nanometres (nm) [63]. More narrow definitions consider only particles smaller than 10-20 nm as nanomaterials because many of the solid material properties drastically change below that size [64]; these changes are called quantum size effects or simply "size effects" [6]. These properties include, at the single particle level, 1) decreased melting points and boiling points, 2) increased dielectric constants, 3) super-paramagnetic properties in ferromagnetic materials, 4) increased surface energies, and 5) changes in light absorbance and reflection properties [64]. The population properties affected by the small grain size are, e.g., increased specific surface area, changes in dispersibility and aggregation behaviour, and increases in the mechanical strength.

Nanomaterials are produced because these properties make them different from bulk materials with the same chemical composition and result in multiple technological purposes [6]. As a downside, nanomaterials are hypothesised to impose different degrees of adverse biological effects [65], such as enhanced permeation and retention in biological membranes [66]. Moreover, the cohesion between nanoparticles significantly increases with increases in the specific surface area. This behaviour decreases the handling and applicability of nanoparticles [64].

2.4.2 Manufacture and engineering of nanomaterials

Nanomaterials are produced today in large quantities via several methods based on liquid, solid or gas-phase synthesis. Aerosol technology is an important route for the manufacture of commercial quantities of nanoparticles [67]. Aerosol processes are based on the principles of gas-to-particle or droplet-to-particle conversion. Flame processes are used in the manufacturing of carbon black, fumed silica, pigmentary titania, and optical fibres [19]. The success of this technology is based on the simplicity of the process, purity of the produced materials, and absence of liquid by-products [67]. Aerosol processes are capable of producing a broad variety of materials with good control of product characteristics, such as particle size, shape, chemical composition, and crystallinity [6].

A number of engineering strategies may also be used to control the nanomaterials that originate from both natural and human sources. The engineering strategies have been directed toward a) passive nanostructures, such as coatings, or b) active nanomaterials, such as vehicles for the targeted delivery of drugs [67]. Passive coatings may function simply by reducing the particle surface free energy to enhance dispersion or act as electrochemical or physical barriers between particles and the environment [68]. Active designs may alter their behaviour in response to changes in pH or temperature [69].

Due to widespread application of aerosol technology in commercial nanoparticle production, more and more people are potentially exposed to nanoparticulates. So far, no epidemiological studies exist on the possible adverse health effects of nanomaterials, partly because of the requirement for long-term studies and a large number of exposed humans [5, 65].

2.5 SOLID STATE PROPERTIES OF NANOMATERIALS AND ZINC OXIDE

2.5.1 Crystalline, polycrystalline, nanocrystalline, amorphous

In a crystalline material, the molecules are arranged in a periodic array (lattice) of repeating unit cells [70]. Perfect crystals rarely occur in nature, and defects in the crystal can occur, e.g., stacking faults, dislocations, and twinning [71].

In materials science, microcrystallinity and nanocrystallinity are terms that are sometimes referred to as synonyms. In this thesis, the term *nanocrystallinity* is used to describe medium-range ordering (0.5-2 nm). *Polycrystallinity* refers to materials that are composed of many single crystallites with varying sizes and orientations [72]. A solid without long-range translational structural order is best described as *amorphous* [73]. Examples of amorphous solids are glasses, polymers or amorphous carbon [74]. However, amorphous materials may possess ordering over distances of 1–10 nm [73].

The dynamics of crystalline particle formation and growth in aerosols is driven by the same processes as particle growth processes in general (see Chapter 2.2). However, the anisotropic dynamics of crystal formation adds many additional boundary conditions to the problem. The growth is fastest on the crystal planes with the highest surface free energy; thus, the shape is determined by the minimum total surface free energy [75].

The crystallinity of a solid material is a relational property, especially for solids that form under nonisotropic temperature conditions. During combustion, a rapid change in the reaction kinetics frequently occurs; under such circumstances the existence of amorphous or metastable forms is likely, particularly if the particles are small [67,76].

2.5.2 Zinc oxide

Zinc oxide (ZnO) is a stable crystalline oxidised form of Zn. ZnO is poorly soluble in water. In industry, ZnO is used in sensors, as a UV-absorber, and as a catalyst [77]. ZnO is known to efficiently absorb some organic species and heavy metals [77]. Bulk ZnO is stable at relatively high temperatures and has a melting point at 1975 °C [78]. Under reducing conditions, ZnO may be reduced to elemental Zn.

ZnO has useful characteristics, such as a large piezoelectric constant, crystal lattice adjustability via the addition of dopants [79], and its electrical conductivity can be easily modified. The properties of ZnO strongly depend on its crystal features, such as aspect ratio, size, orientation, density and exposed faces of the crystal [6].

The crystal appearance, or habit, is a strong indicator of the crystal structure, see Fig. 2.2(a-c). The most stable polyform of ZnO at ambient temperature and pressure is hexagonal wurtzite (hcp) where every Zn atom is surrounded by four oxygen atoms (Figure 2.2(d)). The ZnO crystal is grown in the direction of either of the polar surfaces Zn-ZnO(0001) or O-ZnO(000-1) (Fig. 2.2(b)) [80]. The other sites are non-polar and, therefore, possess lower surface free energy than the polar sites.

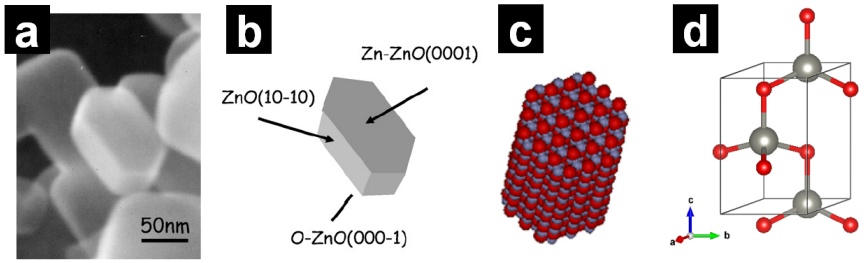

Figure 2.2: (a) ZnO powder particles viewed by SEM [80]; (b) Hexagonal shape of a ZnO single crystalline particle, side faces marked with Bravais-Miller notation [80]; (c) Atom model of a ZnO crystal with hexagonal crystal habit [80]; (d) Atom model of ZnO unit cell, build with Vesta 3.16 [81].

ZnO is reactive for different species, and may dissociatively adsorb small molecules (e.g., CO, CO_2, NH_3, H_2O and H_2S) [29, 80] into a ZnO crystal [80]. Moreover, the ZnO surface can efficiently catalyse the formation of carbonate species from CO and CO_2 [29, 80] as well as sulphate species (SO_3 and SO_4) from S and SO_2 [82]. Similar behaviour is also found for chlorine [83]. These surface mediated processes may lead to transfomation of ZnO to zinc carbides, sulphides or chlorides; the transformation may be complete or partial, depending on the particle surface-to-volume ratio and the concentrations of the reactants [30].

In biomass fuels, zinc is bound in the woody constituents in various forms, such as elemental Zn, ZnO and organically bound Zn [84], and is released as gaseous Zn at reducing, high temperature pyrolysis conditions. In combustion gaseous Zn is oxidised to ZnO, which similar to most transition metal oxides has a lower vapour pressure than its corresponding elemental form [75].

Natural untreated wood products contain approximately 5-210 mg Zn per kg of dry fuel [57]. The highest Zn concentrations in untreated woods can be found in fuels containing bark, which in general have high contents of ash forming species [52]. Jones *et al.* [84] have recently reviewed the zinc contents of other materials used as fuels for power and heat production. Of the various combustible waste products, Zn concentrations comparable to those used in this study (Papers **III-IV**) were reported for recovered waste wood (70-1000 mg kg^{-1}), sludge (2000 mg kg^{-1} in average), municipal solid waste (3000-4000 mg kg^{-1}), and other waste derived fuels, such as plastics, papers and textiles (approximately 1100 mg kg^{-1}) [84].

2.6 HEALTH EFFECTS OF PARTICLE EXPOSURE

2.6.1 Adverse health effects via a pulmonary route

As described in the previous section, particles are frequently present as a mixture with gaseous and semivolatile species in the atmosphere. In polluted air, the particle number concentration can be higher than 10^4 cm^{-3} [23]. The main adverse effects of particulate

air pollution are related to respiratory and cardiac illnesses and to reduction of the life expectancy in humans [10,20].

The importance of particle size is emphasised due to the size selective function of the lung. Inhaled particles target different parts of lungs, depending, e.g., on the aerodynamic diameter of the particles [85]. The particles within the size range between 10 and 2.5 μm remain in the upper and lower airways, whereas PM_1 are able to enter deep into the alveolar region. The fraction of particles that is not exhaled is retained and may interact with the tissue.

The deposition of particles into the respiratory tract may lead to systemic effects in the human vasculature due to the release of inflammatory cytokines into the blood stream [20]. The inflammatory potential of particles may vary with chemical composition, size, crystalline structure and solubility of the particles, or due to surface bonded agents (e.g., bacteria and pollen) [63,85].

2.6.2 Mechanisms of particle induced toxicity

The main toxicological mechanisms associated with particle induced biological effects are inflammation, oxidative stress and genotoxicity but also cytotoxicity results in damage in the cardiorespiratory systems [86]. Tissue and cell culture analyses suggest a role of reactive oxygen species (ROS) and oxidative stress in the generation of the inflammatory responses and cytotoxic effects [87].

The ability of PM to oxidise target molecules, defined as its oxidative potential, has been proposed to be a more biologically relevant factor than PM mass for particle-induced toxicity [88]. Small particles have more surface molecules per unit mass of material than larger particles, enhancing their electron transfer and surface chemical activity. Indeed, there is a direct relationship between the large specific surface area, ROS-generating capability, and inflammatory effects of ultrafine particles in lungs [63].

Due to the heterogeneity of ambient PM, differentiation between contributors of toxicity of the PM is difficult. Metals in the PM have long been suspected to play a crucial role in particle mediated

lung inflammation; however, the influence of other components has left the question open [89]. More understanding of the structural heterogeneity of particles is required to evaluate the mechanisms of toxicity.

2.6.3 Toxicity of zinc

Zinc is an important trace element and nutrient for animals and plants. Zinc is required for multiple cell functions, such as cell growth, differentiation, RNA transcription, DNA synthesis and cell metabolism [7, 90]. Inside cells it is mostly bound to proteins and certain cell organelles [85]. The cells naturally have developed mechanisms to transport, bind and release zinc whenever it is necessary. The free ionic form of zinc [Zn^{2+}] is quite rare in the cell medium under normal conditions.

The cytotoxicity and inflammatory potential of ZnO particles have been shown to be connected to intra- and extracellular particle dissolution [91,92]. According to the paradigm, the uncontrolled increase of ionic zinc disturbs the cellular homeostasis via a cascade reaction following the loss of ionic stability of the cell [7]. Another mechanism suggested is that oxidation-reduction reactions may occur on ZnO particle surfaces, producing reactive species, such as hydrogen peroxide (H_2O_2) or hydroxyl radicals (OH•) [93, 94]. In that way, no dissolution of particles was needed for oxidative stress injury. Both paradigms are supported by studies where coating ZnO nanoparticles with a more passive material (TiO_2 [95], SiO_2 [96], or PEG polymer chains [97]) has been shown to reduce the ZnO particle toxicity.

There is a very limited amount of information available on the role of zinc in the toxicity of biofuel combustion emissions. Because emission samples are mostly collected as atmospheric mixtures, these studies do not usually sequestrate the sources of pollutants. Such studies are neither able to determine the formation conditions of particles, e.g., the role of the fuel type and the combustion appliance. Therefore, studies of fresh emissions, which have knowledge of these process parameters, are needed.

2.7 THE IMPORTANCE OF STUDYING MORPHOLOGY

Morphology is study of shape, size, texture and phase distribution of physical objects. Because of the quantum size effect, the structure and surface properties are accentuated in the properties of nanomaterials. Therefore, the criteria to evaluate particle toxicity based on morphological properties should be developed [93].

In this study, the primary method for studying morphology was transmission electron microscopy, which can be defined as single particle analysis. Although the resulting information is often qualitative, it is something that cannot be obtained via other methods. As a drawback of this approach, the statistics of the analysis will essentially be poor which reduces the possibilities for generalisation of the observations but may avoid incorrect conclusions based on the bulk data.

For example, the particle size has implications on the transformation, transport, and optical properties of particles. Morphology has an indirect but important effect on the particle size measurement: the sphere is the only object whose size can be defined by a single size parameter – its diameter [16]. Most particles are not spheres, and have various densities. Non-spherical particles have in general larger surface areas than aerodynamically equivalent spheres. The shape parameters can be evaluated using EM.

Occasionally, observations of the external crystal symmetry may reveal to what system it belongs: cubic, hexagonal, or tetragonal, to name a few [74]. In addition, the growth of particles with well-defined crystal habits is often promoted by defects, such as stacking faults. In nanomaterial engineering, these defects may affect the physical properties of the material.

In addition, electron microscopy analysis provides structural information related to the crystalline order in the material. Polycrystalline structures and, e.g., nanocrystalline soot, can be investigated using EM diffraction and image analysis techniques [98].

Moreover, by observing the grade of sintering, primary particle size or dendrite formation, the conditions during particle forma-

tion and growth can be deduced. The morphology may give information on which processes were the rate-determining steps in the growth and maturation of a particle. For example, a high coalescence rate may manifest as a large primary particle size.

Furthermore, the transformation of particles may be observed. By atmospheric aging, several alterations of particle composition and physiology occurs, e.g., heterogeneous chemical modifications with nitric acid and sulphuric acids [99]. Normally both the size fraction and the particle composition change. For example, studies of polluted air show that K- and S-rich particles tend to scavenge any fine insoluble aerosol particles [99]. Additionally, dynamic changes can occur under the beam, e.g., vapourisation, adsorption, aggregation and phase change.

For small groups of particles, for example in dispersions, the state of aggregation and dispersibility can be observed [87]. Moreover, the properties of coating thicknesses and surface properties of the engineered particles may be resolved [96]: studying particle morphology can aid in the final adjustment of the synthesis parameters when accurate properties of the final particles or coatings are needed.

3 Experimental methods

3.1 BIOMASS COMBUSTION APPLIANCES

Combustion experiments were performed in the emission research laboratory at the University of Eastern Finland, Kuopio. Two combustion appliances were used for the combustion of different woody fuels. A schematic diagram of the measurement setups used in Papers **I**, **III** and **IV** is shown in Fig. 3.1. The minor differences between the setups are denoted with symbols.

In Paper **I**, the fuel was approximately 30-mm wood chips from both bark and stem wood material from spruce and typical Finnish broadleaved trees. The zinc concentration of the wood chips was 35 mg/kg. In Papers **III** and **IV**, pure shavings and sawdust from pine stem wood was used as the raw material in the pellets. The material was first ground and then mixed with elemental zinc powder at various concentrations or left unaltered. After mixing, the materials were pelletised. The zinc contents per 1 kg of the fuel were 11, 170, 480 and 2300 mg kg^{-1}. The concentration range corresponds to previous studies [57, 84]: the smallest naturally occurring concentration of Zn bound in wood and the largest for the fuels used in waste incineration, see also Chapter 2.5.2.

The fuel was fed into the combustion unit (Fig. 3.1) using either a moving step-grate combustion reactor (Paper **I**) with adjustable air staging and an adjustable velocity fuel feed or a pellet boiler (Papers **III** and **IV**). The exhaust from the combustion units was led to a stack, where the sampling for measurement and collection occured.

The dilution of the particle samples was performed using porous tube diluters (PRD) and ejector type diluters (ED). The dilution system used has been validated via several previous biomass combustion studies [100–104]. The purposes of an efficient dilution system in a reaction experiment are (1) quenching of the chemical reactions

and agglomeration, (2) decreasing the concentrations to a specified level for measuring and collecting devices, (3) cooling of the emission gases to ambient level, and (4) minimising particle losses on the walls or ensuring good mixing of the sample with dilution air.

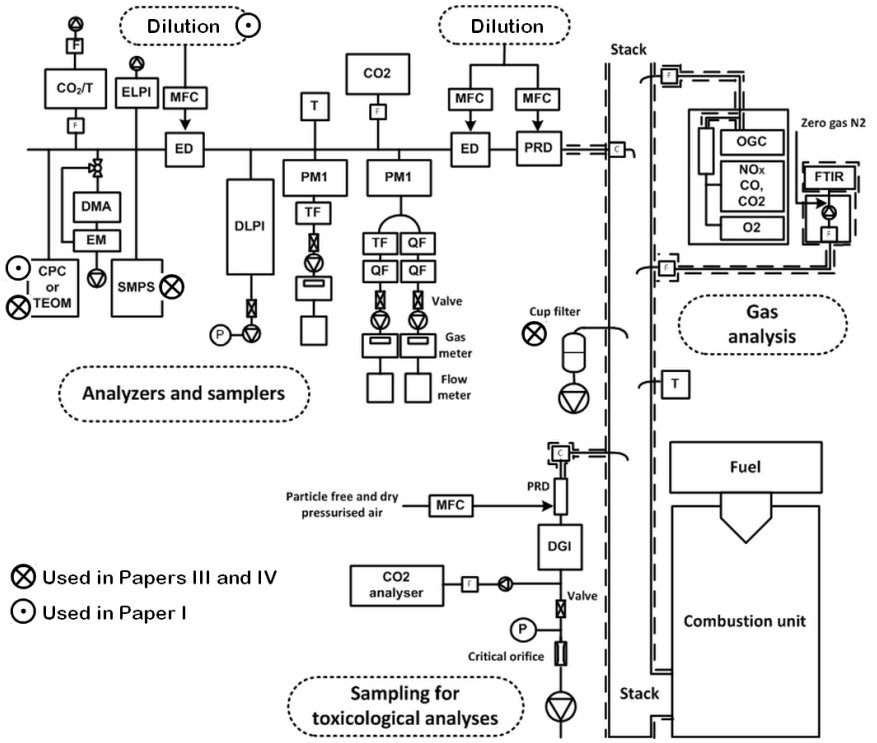

Figure 3.1: Schematic of the experimental setups in combustion of woody fuels in Paper **I** *(⊙), and in Papers* **III** *and* **IV** *(⊗). Abbreviations: T =Temperature control; ELPI = Electrical low-pressure impactor; P = Pressure sensor; DLPI = Dekati low-pressure impactor; MFC = Mass flow controller; DMA = Differential mobility analyser; TEOM = Tapered element oscillating microbalance; TF = Teflon (PTFE) filter; CPC = Condensation particle counter; QF = Quartz filter; OGC = Organic gaseous compounds; C = Cyclone; FTIR = Fourier transform IR-analyser; F = Filter; DGI = Dekati gravimetric impactor; PRD = Porous tube diluter; CO, CO_2 = Carbon oxide analyser; ED = Ejector diluter; NOx = Nitrogen oxide analyser; PM_1 = PM_1 impactor; O_2 = Oxygen analyser.*

Temperatures were monitored continuously from the flue gas and particle sample lines using K-type thermocouples (marked with T in Fig. 3.1). Sensors for CO_2 were used before and after the dilution steps (marked with CO_2 in Fig. 3.1). The coarse particles (cutoff aerodynamic diameter at 1 μm) were removed using cyclons or filtration. A varying assembly of devices used for the characterisation of the emissions and the collection of the PM for physico-chemical and toxicological analyses was used (Fig. 3.1). The corresponding methods are described in Chapter 3.3.

3.2 FLAME SPRAY SYNTHESIS

In Paper **II** a flame spray pyrolysis (FSP) was utilised for combustion of precursors solved in ethanol. The setup is shown in Figure 3.2 with the measurement devices marked with acronyms, more closely defined in Chapter 3.3. The precursors for the flame synthesised composite particles in Paper **II** were potassium acetylacetonate, dimethyl sulfoxide, and zinc acetate dihydrate.

The precursor solution was dispersed using oxygen gas and ignited. The continuous feed rate of the precursor was 1 ml min^{-1}. The oxygen flow rate was 2 l min^{-1}. A flamelet of premixed methane and oxygen in stoichiometric ratio was used to ignite and maintain the main flame. A flow rate of 5 l min^{-1} of particle free, dry sheath air was added before the flow reactor inlet to minimise losses in the reactor walls.

The combustion products were fed into a 80-cm-long silicon carbide flow reactor tube (inner diameter 28 mm) heated to 1000 °C. The dilution of the particle samples was performed in three stages using a PRD and two EDs in series, similar to the wood combustion experiments.

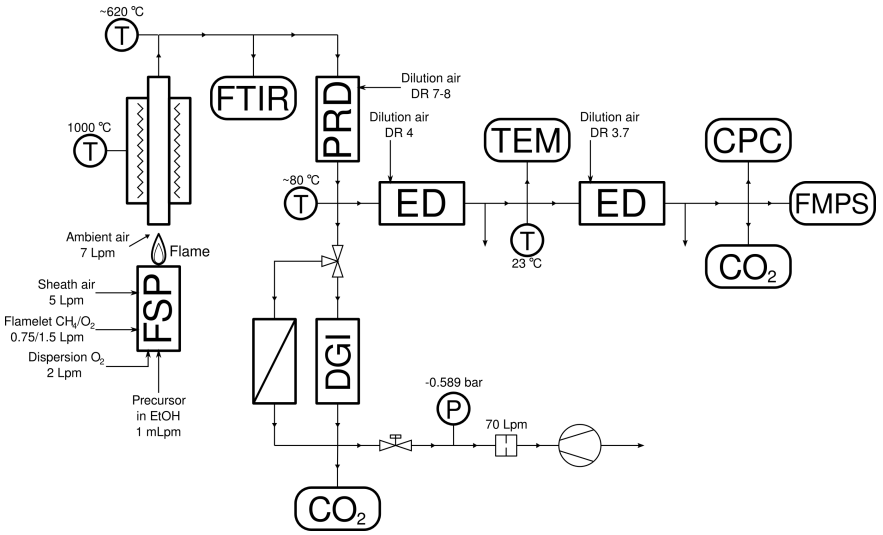

Figure 3.2: Schematic of the flame combustion reactor used for synthesis of pure alkali and ZnO particles (Paper **II***). Abbreviations: FSP = Flame spray pyrolysis; T =Temperature control; P = Pressure sensor; CPC = Condensation particle counter; FTIR = Fourier transform IR-analyser; DGI = Dekati gravimetric impactor; PRD = Porous tube diluter; CO2 = Carbon dioxide analyser; ED = Ejector diluter; FMPS = Fast mobility particle sizer.*

3.3 MEASUREMENTS AND MATERIALS ANALYSES

3.3.1 Particle number and mass size distributions

The aerosol number size distributions were determined continuously from the gas phase using a scanning mobility particle sizer (SMPS, Papers **I-IV**), electric low-pressure impactor (ELPI, Papers **I** and **III**) and a fast mobility particle sizer (FMPS, Paper **II**). A condensation particle counter (CPC) was used in Paper **III** to determine the particle number concentration. In addition, a differential mobility analyser (DMA) was used in Paper **I**, in series with a CPC and a TEM sample collector, for size-segregation of the aerosol for electron microscopy analysis.

The aerodynamic mass size distributions were determined from the gas phase using a Dekati low-pressure impactor (DLPI) with greased aluminium foils (Papers **III**) or clean PTFE foils (Paper **I**)

as collection substrates. In Paper **III**, real-time measurement of the particle mass concentration was performed using a tapered element oscillating microbalance (TEOM) monitor.

3.3.2 Chemical analyses

Both inductively coupled plasma mass spectrometry (ICP-MS) and ion chromatography (IC) were used to determine the concentrations of the elements and anions in the PM samples in Papers **I**–**IV**. The samples for both analyses were collected on polytetrafluoroethylene (PTFE) filters. Additionally, the bottom ash sample chemical composition was analysed in Paper **III**. The analysis service was purchased.

An alternative method for determining the concentrations of elements, used in Paper **I**, was proton induced X-ray emission (PIXE). The method was used in Paper **I** to determine the aerodynamic distribution of elements in efficient wood combustion PM_{10}. The analysis service was purchased from a certified test laboratory.

PM_1 carbon fractions were analysed using a thermal-optical carbon analyser (Sunset Instruments) with NIOSH Method 5040. The carbon analyser measures the amounts of organic and elemental carbon in the sample. The samples were collected on quartz filters using a validated quartet-filter method [105]. In addition, the amounts of carbonate carbon were estimated according to the NIOSH protocol [106].

A gas-chromatograph mass spectrometry analysis of polyaromatic hydrocarbon (PAH) compounds was used in Papers **I**, **III** and **IV**. The quantification limit of a compound was 0.1 ng mg^{-1}, but as the analysis was performed in multiple phases, the total amount of sample needed for analyses was high, approximately 10 mg.

3.3.3 Gas emission analyses

Gaseous samples were measured and analysed directly using a Fourier transform infrared (FTIR) spectrometry gas analyser (Gasmet Technologies), including a separate O_2 analyser. FTIR is a

technique that provides information about the chemical bonding or molecular structure of materials based on their absorption of light at infrared frequencies. The detector cell is heated to 480 °C. In Paper **III** the analysis was used for the measurements of NO_x, CO, CO_2, H_2O, SO_2, HCl and 28 volatile organic compounds. In Paper **II** the main combustion species of the reactions, NO_x, CO, CO_2, H_2O, SO_2, were determined.

3.3.4 X-ray diffractometry

The crystalline phase of materials were studied with X-ray diffractometry (XRD, Bruker D8 Discover, Cu Kα source, 40 kV, 40 mA) in Papers **II**, **III** and **IV**. The data were analysed using the Topas 3 software. The crystal sizes were calculated based on the fundamental parameter approach and the Rietveld method [107]. The crystal aspect ratio was obtained from the crystallite sizes determined separately for the diffraction peaks parallel and perpendicular to the crystallite growth direction.

The XRD is based on the ability of a crystalline sample to scatter coherent emissions of X-rays. XRD can be used to determine the orientation of a single crystal or grain, find the crystal structure or identify different polymorphs of a material, and measure the size and shape of small crystalline regions [44]. The amount and homogeneity of the analysed material affects the precision of the measurement and clarity of the results. A sufficient amount of a powder sample for XRD analysis is greater than 10 mg. Therefore, it is a bulk analysis by nature, identifying the major crystalline phases only. The peak broadening caused by particles with nanocrystalline structural order reduces the degree of accuracy of the method [108]. The accuracy may also be reduced by diffraction peak overlapping in multicomponent samples [108]. Both situations are common in multicomponent, fine structured environmental particulate emissions. In this thesis, XRD was used to identify the crystal phase of ZnO in the PM samples.

3.3.5 Transmission electron microscopy (TEM)

In this study the single particle morphological features were studied using field emission TEM (JEOL JEM-2100F), operated at a 200-kV acceleration voltage. An electron microscope consists of an electron gun, electromagnetic lenses, apertures, stigmators, deflectors, and the optics required for image viewing. In addition, the field emission TEM was equipped with analysers enabling the usage of energy dispersive spectrometry (EDS).

Detailed atomic level structure can be measured with TEM because electron wavelengths (0.04-0.008 Å) are shorter than the lattice parameters of crystals [71]. Many TEM techniques are based on the so called thin foil approximation (1-100 nm) that ensures elastic scattering processes where the electron energy is conserved, and thus, the wavelength remains unchanged [74].

The conventional bright field (BF) TEM image is created from the amplitude and phase contrast phenomena and by the interaction of the transmitted electron beam with the solid material [44]. The amplitude contrast is usually enhanced by the exclusion of high angle scattered electrons using apertures.

The coherent elastic scattering of electron waves from adjacent, regularly spaced layer planes is referred to as Bragg diffraction [44]. The diffracted beam direction and intensity are inherited from the lattice structure of the specimen. Both amplitude and phase contrast phenomena occur simultaneously in the transmitted wave.

Diffraction patterns (DP) are obtained in the same conditions as other TEM analyses; however, the magnified image of the back focal plane of the objective lens is observed instead of the image of the sample. In this way, the information about the crystalline properties of the sample becomes available. Selected area electron diffraction (SAED) is a technique where DP are obtained by selecting only certain diffraction angles with an aperture in the imaging column. SAED from small volumes (nanodiffraction) most often results in poorly oriented, weak intensity DP, which reduces the effective use of the technique. The effective use of proper nanod-

iffraction techniques (e.g., CBED) in TEM analysis requires equipment with precise convergent beam illumination and a double tilt specimen holder [71].

Diffraction may be observed directly from the image. Whenever the object is suitably oriented with some of the lattice planes in Bragg condition with the beam, a regular contrast variation, fringing, may occur in the image. Moreover, the operator can selectively accentuate a certain contrast-creating factor in the beam. For example, dark field (DF) TEM is accomplished by blocking the specularly transmitted (central) electron beam, and selecting only a particular Bragg maximum at a certain angle to create high diffraction contrast between diffracting and non-diffracting objects [71].

Energy dispersive spectrometry (EDS) is used to detect the spectrum of characteristic X-rays that are created due to inelastic scattering in the sample [71]. The data are received as intensity spectra at characteristic energy channels in the keV range.

In this thesis, BF TEM and SAED were used to study the size, surface properties, heterogeneous structure, and single crystalline diffraction in the PM samples. DF TEM was used to identify the nanocrystallinity in the samples. EDS was used to identify the elemental composition of the species.

3.4 CALCULATIONS

3.4.1 Real-time gas and particle concentration data

The particle size distributions were either mass concentrations (mg m^{-3}) or number concentrations (# m^{-3}). The values were normalised to a reference condition and oxygen concentration in the dry flue gas. In Paper **III** and **IV**, these conditions were 20 °C, 1 atm and 10 % O_2. In Paper **II**, normal conditions (NTP, 0 °C, 1 atm) and 17 % O_2 were used, and in Paper **I**, the reference values were also in NTP and 10 % O_2. The concentration data were dilution corrected.

Nominal emission (mg MJ^{-1}) was calculated in relation to the energy input (MJ) in the combustion process. The dilution ratio

for all of the diluted samples was calculated based on the concentrations of CO_2 (dry) in raw and diluted exhaust gas, as described previously in Tissari *et al.* [100].

3.4.2 Thermodynamic equilibrium calculations

Thermodynamic equilibrium calculations were used in Papers **I**, **II** and **III**. The method identifies the most probable species in a multiphase system using a method of Gibbs free energy minimisation [26]. A thermodynamic database was used, which contained temperature dependent values of heat capacity, entropy and enthalpy for each species [26].

The aim of the calculations was to obtain information on the inorganic compounds present in the fine particle fraction and rough estimations of the gas-to-particle conversion temperatures of these species in the cooling flue gas. A temperature range of 80-1600 °C was assessed. The calculations were performed in both oxidising (Papers **I**-**III**) and reducing (Paper **III**) atmospheres. In Papers **I** and **III** the concentrations of the ash species were based on the PM_1 analyses, and the concentrations of the gaseous species were based on the analysed gas composition of the flue gas. In Paper **III**, the concentration of Zn was varied in the input, and at the same time, the basic compositional species of the pellet particles remained the same in the calculations. In Paper **II**, the amounts of reactive species were calculated from combustion products using the reactor parameters.

Generally, the method gives good approximations for gas-phase reactions at high temperatures, and it has been found to give plausible results for fine particulate compositions [109]. Sources of uncertainties include the following:

- *Kinetic limitations:* in real systems there are multiple rate-limiting processes, such as chemical reactions and mass transport;
- *Imperfect mixing:* the real distributions of species and products are anisotropic;

- *Non-ideal behaviour of components:* ideal gas approximations do not account for chemical or physical reactions between species but are described solely by the pressure, temperature and volume variables of the surrounding gas;

- *Too many variables:* combustion aerosols are composed of tens or hundreds of species, and only the main components are used in the model.

In general, the species, which have low concentrations and are chemically relatively inactive, can be left out of the system; however, for example, the vast amount of different organic species cannot be treated using a thermodynamic approach, and therefore all effects of those species are omitted. The chemical species libraries are of high quality and increasing. Unfortunately, information for some important species may be missing. The behaviour of some components, for example phosphates, is also very unpredictable. The limitations of the method in modelling environmental gas-phase systems are discussed in more details by [53, 60, 110].

3.5 STUDY DESIGN FOR TOXICOLOGICAL STUDIES

The mouse macrophage cell line used in this study (Papers **II** and **IV**) is a cell model for active defence mechanisms against particulate emissions in the lungs. The lung functional purpose is to provide a large alveolar surface area for gas exchange. The airway epithelium provides a physical barrier between the body and the external environment, prohibiting the entry of water, small particulates, and microbes [89]. It also has active clearance of materials through a mucociliary pathway and active defence cells, such as macrophages. Inflammation occurs when the defence cells or epithelial cells become activated by external stimuli to release inflammatory mediators, such as TNF-α [85].

In Papers **II** and **IV**, mouse RAW264.7 macrophages were exposed to PM samples according to procedures validated in previous publications [111, 112]. The cells cultured in 6-well plates were

Table 3.1: Toxicological end points of the in vitro *experiments.* [a]

Paper	Sample name	Dose μg/ml	Markers
II	ZnO	15, 50, 150, 300	PI-exclusion assay, cell cycle, ROS, TNF-α
	K_2SO_4	15, 50, 150, 300	
	$K_2SO_4 + Zn$	15, 50, 150, 300	
	K_2CO_3	15, 50, 150, 300	
	Wood PM	15, 50, 150, 300	
III, (**IV**) [b]	Reference pellet (Native)	15, 50, 150, 300	PI-exclusion assay, cell cycle, SCGE, ROS, TNF-α, MIP-2
	Zn170 (Zn-low)	15, 50, 150, 300	
	Zn480 (Zn-medium)	15, 50, 150, 300	
	Zn2300 (Zn-high)	15, 50, 150, 300	

[a] Abbreviations: PI, propidium iodide; SCGE, single cell gel electrophoresis; ROS, reactive oxygen species; MTT, 3-(4,5-dimethylthiazol-2-yl)-2,5-diphenyltetrazolium bromide; TNF, tumour necrosis factors; MIP, macrophage inflammatory proteins.

[b] The particle generation and characterization was done in Paper **III**, and the toxicological analyses in Paper **IV**. Sample names used in Paper **IV** are in the parentheses.

exposed for 24 h to four doses (15, 50, 150 and 300 μg ml^{-1}) of particles from each situation. The exposures of the cells were carried out in three independent experiments, which included the blank substrate, water and DMSO (0.3 % v/v at dose 150 μg ml^{-1}) control.

The analysed toxicological end points are listed in Table 3.1. The production of proinflammatory cytokines, tumour necrosis factor alpha (TNF-α, Papers **II** and **IV**), and macrophage inflammatory protein (MIP-2, Paper **IV**) were analysed from cell culture medium using commercial ELISA kits. Particle-induced effects on the cell cycle, the total number of propidium iodide (PI) positive cells (PI-exclusion assay), and the intracellular accumulation of reactive oxygen species (ROS) (Papers **II** and **IV**) were analysed using flow cytometry. In addition, genotoxicity was assessed in Paper **IV** by the alkaline single cell gel electrophoresis (SCGE, or comet) assay.

The measured responses were compared to the control and the corresponding blank samples with regard to the particle doses. All

of the measured values were first analysed using Levene's test for equality of variances. The results from the SCGE, PI-exclusion, cell cycle and ROS analyses were evaluated using the non-parametric Kruskal-Wallis test (n = 3). Dunnett's test was used for analysis of the data from the production of the inflammatory mediators (n = 6). ANOVA and Tukey's post hoc test were used in the analysis of differences between the results. Differences were considered to be statistically significant at $p < 0.05$.

4 Results and discussion

4.1 REVIEW OF PAPERS

In Paper **I**, the physical and chemical properties of biomass combustion particles formed in different combustion conditions were studied. The formation of particles was described, and the possible effects of the combustion conditions on the particle morphological features were discussed. In particular, condensation of organic matter on particles caused significant variation in the appearance of both ash and soot particles. The results indicate that the properties that may affect both the atmospheric behaviour and toxic potential of the particles are dependent on both the fuel and the conditions during the combustion process.

In Paper **II**, nanoparticles composed of potassium, sulphates and zinc were synthesised, and their toxicity was tested *in vitro*. In addition, the toxicity was compared with the PM_1 from the efficient combustion of wood chips studied in Paper **I**. The PM_1 samples were cytotoxic and caused cell cycle arrest and ROS production in the macrophage cells when the particles contained zinc. Moreover, potassium sulphates and potassium carbonate did not induce toxic responses. The results indicate that more attention should be paid to the contents of volatile trace metals in biomass fuels.

Paper **III** is a thorough study of the formation and properties of the emissions, both gaseous and particulate, in pellet combustion when different amounts of elemental zinc were added to the fuel. As a follow-up, the role of zinc enrichment in the PM_1 on various toxicological end points was studied in Paper **IV**. For this thesis, the most important observations made in these two studies are: 1) Zn is released with high efficiency from the fuel, and a significant part of it is enriched in PM_1; 2) at high concentrations of zinc in the fuel, the equilibrium morphology of the resulting ZnO particles approaches that of the engineered, pure ZnO nanoparticles, such as those studied in Paper **II**; and 3) the toxicological responses evoked

by the PM_1 with increasing zinc concentration were similar to those of pure ZnO nanoparticles and PM_1 in Paper **II**.

4.2 PARTICLE FORMATION IN BIOMASS COMBUSTION IN VARIABLE CONDITIONS

In Paper **I**, wood chips were combusted in conditions under which the completeness of the combustion could be altered by adjusting the air staging and fuel feed. Characteristics of the near-optimal combustion were low mass emissions and a high number of small (ultrafine) particles that had low carbonaceous contents due to complete combustion. The less-optimal ("intermediate" in Paper **I**) combustion produced higher gaseous emissions, and the mass emission and median size of the particles were increased due to increased release of soot and particulate organic matter. The least-optimal (or "smouldering" in Paper **I**) combustion generated even higher mass emissions of soot and particulate organic matter.

For single particle TEM analysis, the particles were sampled from the exhaust gas as size-classified samples at 40 nm, 80-100 nm, 150-300 nm, and as non-classified samples. The classification was used for direct observation of the different size modes, hypothesised to be composed of particles with different chemical and morphological properties. The particle morphological features and composition in wood chip combustion PM_1 were heterogeneous, even in the near-optimal combustion conditions, and particularly when the combustion conditions were not optimal. In the following sections, 4.2.1–4.2.3, the main results from Paper **I** are presented.

The main conclusion of Paper **I** was that morphogenesis of the particles in PM_1 is much more complicated than the bulk average values show. The size, mixing state, chemical composition, heterogeneous structure, and amount of organic material in fresh emission are all features that affect the fate of the particles in atmospheric conditions and when inhaled. The wetting properties and metal oxide phase state also directly affect the bioavailability of these particles and, therefore, are of high toxicological importance.

4.2.1 Mixing state of the particles

The ultrafine particle size mode was composed mainly of inorganic ash species, which was the only size mode produced during the near-optimal combustion, indicating complete combustion conditions. The less-optimal and least-optimal combustion conditions produced large amounts of soot and particulate organic matter with number size distribution medians in the accumulation size mode.

The number size distributions and the observed chemical and morphological speciation indicated that the fine soot and ash particles had separate formation routes; the conditions where primary soot particles were emitted from the flame led to a high agglomeration rate of the primary soot, and particles transferred directly to the accumulation size mode. The majority of inorganic vapours went through a growth process initiated by nucleation, coagulation and condensation, which led to particle transfer primarily in the ultrafine particle size mode.

The external mixing was most clearly observed by comparing the size-selected, ultrafine fraction. Internal mixing occured through several mechanisms discussed in Paper **I**: first, the more numerous, smaller ultrafine ash fraction was transferred via agglomeration to the accumulation mode whenever soot particles were present (that is, in incomplete combustion conditions), and second, soot adsorbed inorganic species with higher volatilities from the gas, including potassium and sulphur.

In addition, both soot and ultrafine ash particles were found internally mixed with organic species, which were produced in incomplete combustion conditions. The bulk chemical analyses quantified the organic contents in the PM_1; concurrently, the TEM analysis showed visible changes in the particle surface structure, size and shape in all size classes. As an example, Fig. 4.1(b) shows the amorphous, low-volatility organic mass filling the void spaces in soot agglomerates, which were sampled during a CO-emission event. More stable phases of the incomplete combustion conditions produced more dendritic soot with coarser surface Fig. 4.1(a).

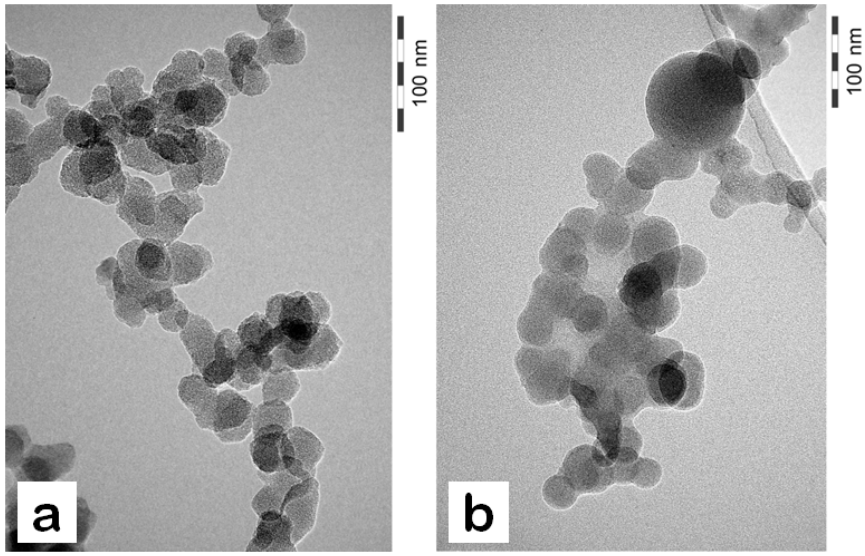

Figure 4.1: Accumulation of organic material on soot particles in incomplete combustion of wood chips. The sample in (b) was collected during a CO-emission event, which can be connected to release of organic aerosols in the exhaust. The CO-emission events were short when compared with more stable phase of combustion, which produced more dendritic soot (a). Published in Paper **I**.

Imaging of the particles does not give a complete picture of the large amount of semi-volatile species truly present in the particulate emissions, which was also discussed in Paper **I**. Therefore, morphological classification of the organic particulate matter is more or less useless. In the current study, this classification was not even attempted, but the strong message was that the contribution of semi-volatile and low-volatile organics affect all of the central morphological features (shape, size, and surface structure) and surface chemistry of the primary emissions, which are important for the particle-induced effects in the environment and for health.

The mixing state of the different particle size fractions has another important consequence: the transfer of ash particles from the ultrafine mode to the accumulation mode may reduce their bioavailability, i.e., the degree to which the substances become available in

lung tissue. In near-optimal combustion, when the soot formation was low, the small ash particles remained in the ultrafine particle fraction. This size mode is believed to be potentially dangerous due to the small size, large surface area to mass ratio, deep airway penetration, and ability to be retained in the lung [8]. In incomplete combustion cases the particles were partially "filtrated" into the larger particle fraction. When inhaled, large particles are mainly deposited in the tracheobronchial region of the respiratory tract [33] and, therefore, more easily eliminated by the defence mechanisms of the human body.

4.2.2 Soot structure

The crystalline order of carbon atoms in soot particles was found to vary from random (amorphous) to medium-range ordering (Fig. 4.2 a-c) in Paper **I**. Medium- to long-range crystalline order of carbon atoms, often reported, e.g., in diesel fuel derived soot [113], were not observed. At best, medium-range ordering was visible at high magnification (Fig. 4.3(a-b)). The various condensed organic species, whenever identified, were amorphous.

Low flame temperature yields amorphous carbonaceous products [42]; consequently, the flame temperature sets the basic boundaries to the resulting structures. The fuel also has an important role in the structure of soot. The amount of disorder within diesel soot nanostructures increases as the oxygen content of the fuel increases [46]. In biomass, the carbon is bound in woody constituents, such as lignin, cellulose and hemicellulose, which may have different oxidative properties than the shorter hydrocarbons found in fossil fuels [35]. It has been suggested that the oxygen-bearing components affect the sooting process, reflecting the graphitising behaviour [114], and making the soot more reactive and, for example, more absorptive for many species [40]. These properties are known to have direct implication on, e.g., the hygroscopicity and cloud formation ability of soot in the atmosphere [35,49].

In some instances, nanocrystallinity in soot can be distinguished

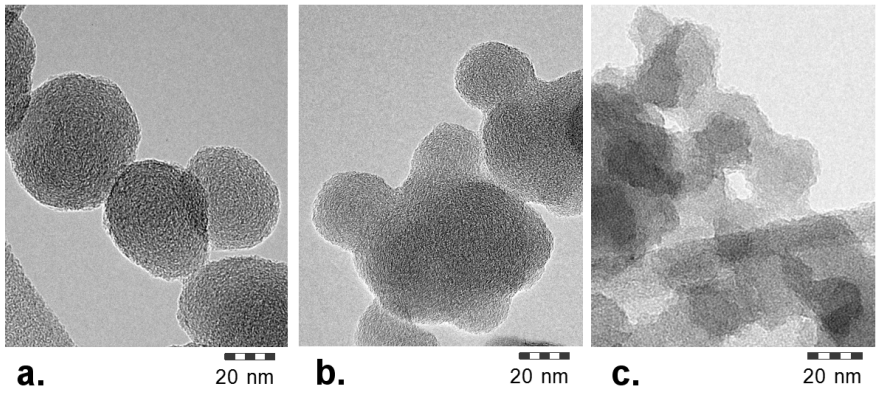

Figure 4.2: Different forms of carbonaceous particles, defined as soot: (c) short-range ordered (nanocrystalline); (d) amorphous and sintered; (e) sintered and surface covered with organic species.

from the amorphous counterpart with dark field imaging. In Fig. 4.3(c), by selecting a single sum wave in an arbitrary direction and blocking the central sum wave, the contrast between the diffracting and non-diffracting volumes were enhanced. The bright field image in Fig. 4.3(d) contains the same information, but it is dominated by the central sum wave, which mainly shows the mass-thickness contrast of the target, and the individual crystallites are not observed.

Soot contains small amounts of inorganic species [115], which is supported by the TEM-EDS analyses in Paper **I**. One probable reason is that soot adsorbs inorganic species from the surrounding gas on the surface of the soot. However, it is currently not known whether some ionic species contribute to the reactions forming primary soot structures already in the flame [43]. Keeping in mind that biofuels contain more ash forming ionic species, it is a possible scenario explaining some of the chemical and structural differences between biofuel soot and, e.g., diesel combustion soot [43]. This proven, global atmospheric modelling would help better identify different sources of soot.

These observations are in line with previous studies, which emphasise the role of fuel and combustion conditions in the struc-

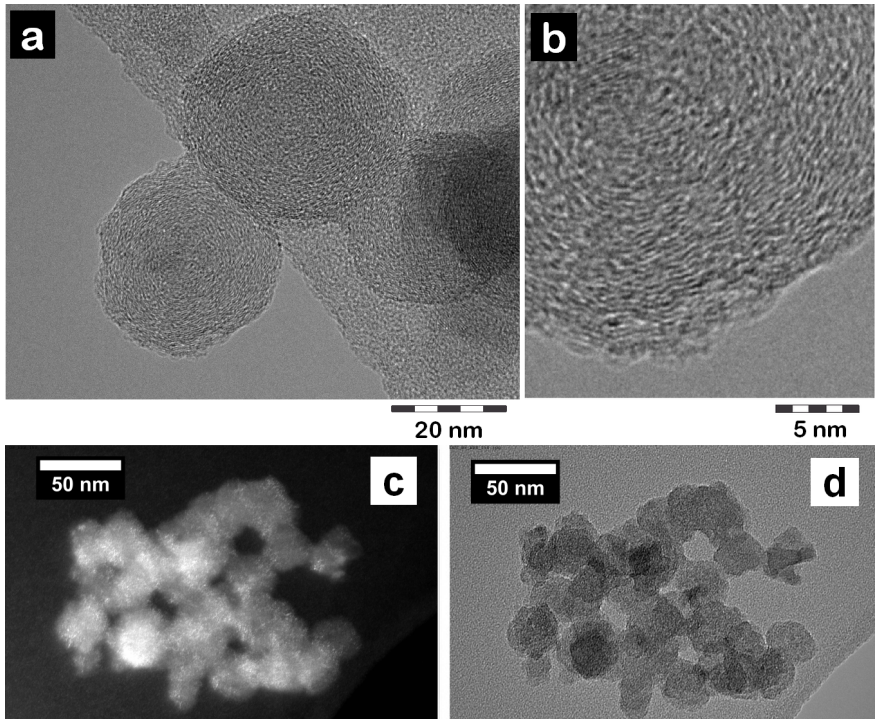

Figure 4.3: (a-b) Soot nanostructure, imaged at high magnification from a primary soot particle on top of a hole on amorphous carbon collection substrate; (c) dark field, and (d) bright field TEM images of a soot particle.

tural formation of soot. In the future, more information on the soot properties could be gained deductively through structural analysis of soot prepared using, e.g., high temperature annealing. Thermogravimetric on-line analysis of volatile species leaving the sample would add value to the analyses.

4.2.3 Inorganic particles

The inorganic fraction of the PM_1 in Paper **I** was composed mainly of alkali salts. The observed morphological features of the primary ash particles in PM_1 indicated that primary growth occurred via nucleation, agglomeration (sintering) and condensation in the cooling heterogeneous gaseous environment.

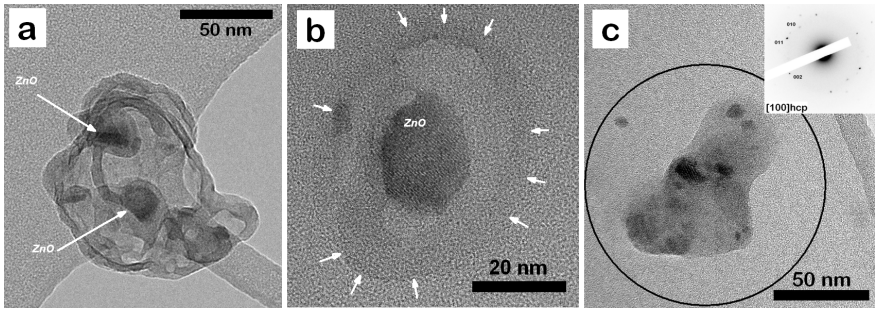

Figure 4.4: Stratified structure of ash particles: (a) marked with white arrows two zinc oxide (ZnO) nuclei inside alkali cover; (b) single ZnO nucleus, formerly covered by higher volatile species, of which a low contrast "coffee stain" ring, marked with white arrows, remained. The weak amplitude contrast, forming regular fringes located inside the ZnO nucleus, is due to coherent elastic scattering, and confirms the single crystal phase of the particle; (c) selected area diffraction of a multicompose ash particle. The diffraction pattern (DP) in the inset matches with the hcp structure at the [100] zone axis. The selection of the diffracting area, marked with a black circle, is constrained by the size of the aperture. The colormap of the DP is inverted to enhance the visibility of the weak spots origin from a small diffracting volume.

In general, the ash particles had a stratified structure: the first condensing nuclei were typically composed of species with lower vapour pressures than the upper, more volatile layers. The stratified structure is illustrated in Fig. 4.4 with two examples, imaged under typical conditions where the sample has been already damaged by irradiaton. Similar to the majority of the organic species, many of the light inorganic elements sublime when introduced to the low-pressure conditions present in TEM and heated by the electron beam [116]. In such circumstances, the heterogeneity of the particles is revealed by their evaporation behaviour, as observed in Fig. 4.4(b).

The ash fraction was composed mostly of Cl, SO_4, K, Na, and Zn. Fig. 4.5 shows that the ash fraction of near-optimal combustion PM was mostly found in the PM_1, and the composition of the particles was size-dependent, determined using a DLPI-PIXE analysis. The ultrafine size mode is typically formed via nucleation-condensation process. Possible equilibrium speciation of the main inorganic cations in the PM_1 was calculated (Fig. 4.6). In particular,

the observations supported the speculations that ZnO generate the first condensation seeds for other species in the cooling gas environment [61].

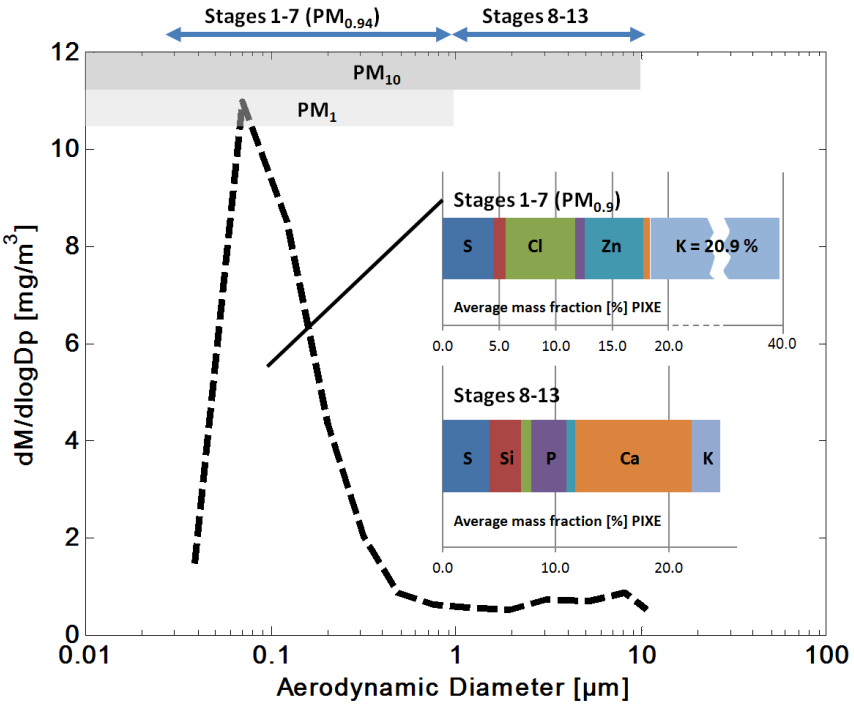

Figure 4.5: The PM_{10} inorganic composition dependence on the particle aerodynamic diameter as determined by PIXE analysis for 13 DLPI stages. The data are for particles produced in efficient combustion of wood chips. Dashed line: mass size distribution (dM/dlogDp, mg/m^3), determined with the DLPI. Colored stacked bars: mass fraction, averaged within stages 1-7 ($PM_{0.9}$) and stages 8-13 (aerodynamic diameter 1-10 µm). Published in Supplementary material of the Paper **I**.

In the TEM analysis, the solid state of ZnO could be directly confirmed only if the nuclei were large enough, as in Fig. 4.4(b-c). The reality was that, in most cases, the occurrence of elemental zinc could be identified only with the EDS. The spatial distribution of Zn was even more difficult to confirm, mostly due to the small

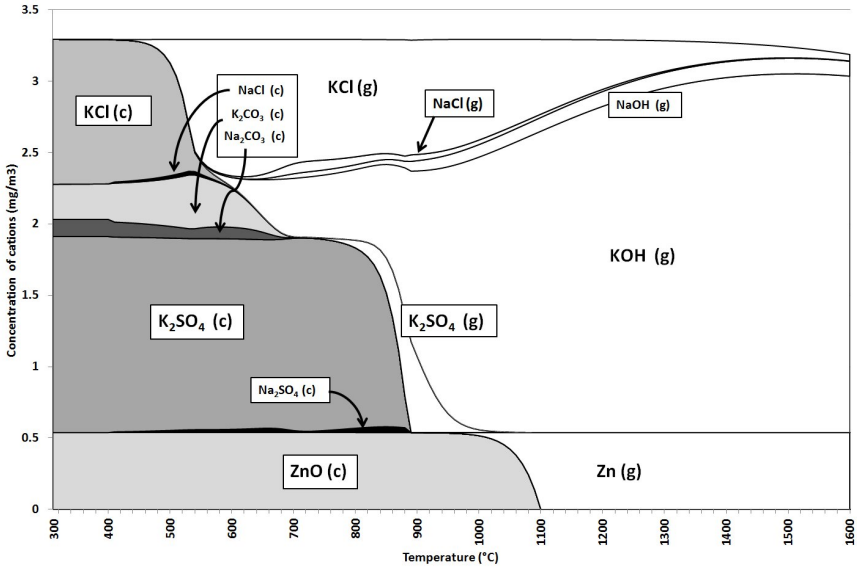

Figure 4.6: Calculated thermodynamic equilibrium between gases and condensed species at various flue gas temperatures. The input species were K, Na, Zn, Cl, SO_4, CO, CO_2, O_2, H_2O, and N_2 in ratios which were determined at the oxidizing conditions in combustion of wood chips. The results are shown as mass concentration of cations. Published in Paper **I**.

size of the nuclei. Because the dark-field TEM is sensitive to short-range crystallinity within the nanometre size particles, it was used to gain qualitative information about the spatial distribution of the crystalline Zn in Paper **I**.

An example of the method is shown in Fig. 4.7: ash particles are imaged in both bright field and dark field illumination conditions. The location of large polygonal shaped crystallites can easily be observed by their diffraction contrast at different angles (a:c, d:f). The same applies to some smaller crystallites in (a), which are absent in (c). There are large numbers of small speckles (d-f), which create contrast via both diffraction (d, f) and mass or thickness (e). It is likely that not all of these crystals are composed of Zn. However, some of the small nuclei were found to be unstable enough to go through changes, such as crystal growth, when heated with the

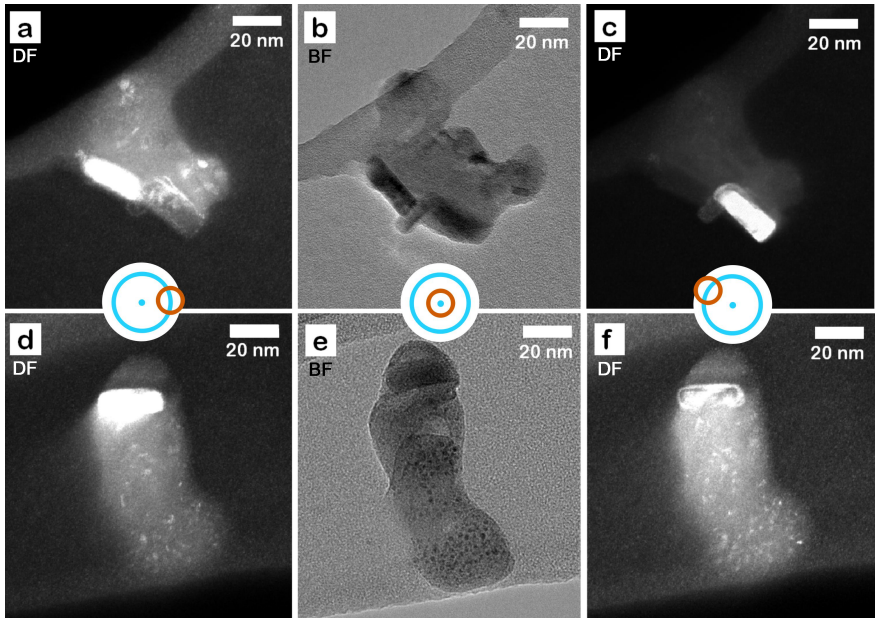

Figure 4.7: Ultrafine ash particles, imaged in (b,e) bright field illumination conditions, contrast formed mainly by the mass and thickness of the sample, and in (a,c,d,f) dark field illumination conditions, where the contrast is mainly formed by the diffraction to an (arbitrary) angle, selected by the objective aperture. The location of aperture relative to the center maxima (blue spot) and the diffraction ring (blue circle) is illustrated with a brown ring.

electron beam. Occasionally these changes resulted in the formation of larger ZnO crystallites.

These types of dynamic changes are extremely difficult to quantify. To date, however, spatial distribution analysis of Zn has not been conducted before at any level for biomass combustion derived ultrafine particles. The results are emphasised here because of the importance of the matter: Because dissolution is one of the key parameters critical to ZnO toxicity [117], the size, distribution and solid phase of the metal containing nuclei, as well as those of the containing matrix, are just the parameters that should be studied more. In the future, this information would be valuable when combined with studies of the solubility behaviour and, finally, with studies of the time and dose-dependent toxicities of the particles.

4.3 PARTICLE FORMATION IN BIOMASS COMBUSTION WITH VARYING ZINC CONCENTRATIONS

In Paper **III** woody pellet fuel with different amounts of added Zn was combusted in a small-scale pellet burner under optimal combustion conditions. The reference case did not contain any added zinc. Moreover, one experiment in less-optimal combustion conditions was carried out. The two highest zinc concentrations of the fuels corresponded with those in waste incineration and nanomaterial engineering. The lower values corresponded with the literature values for pure stem wood fuels and fuels containing bark.

The main results from Paper **III** concerning the particle formation and morphology are 1) zinc is released efficiently from fuel and enriched in the fine particle fraction; however, at low fuel Zn concentrations it can remain in the bottom ash. 2) The structure and phase state of zinc in the PM was dependent on the Zn content in the fuel, and 3) the equilibrium morphology of particles formed from high Zn-content fuel approaches that of the engineered ZnO nanoparticles, such as those studied in Paper **II**.

The release of zinc from fuel to flue gas was found to be effective (over 90 %) and lead to the enrichment of zinc in the PM_1. In addition to Zn, the PM_1 contained 43-67 % of other ash species composed of potassium, sulphate, chlorine, sodium and carbonate. The particulate OC and EC were low, except in the case of less-optimal combustion. In general, the gaseous CO emissions were low, but the addition of zinc into the fuels lowered the CO emissions up to 45 %, regarded as a catalytic effect.

The materials analysis using XRD and TEM showed that the increasing Zn content of the pellets resulted in an increase in the size of the crystalline wurtzite (hcp) phase ZnO particles. For the doped samples, from the lowest Zn concentration (Fig. 4.8(b)) to the highest (Fig. 4.8(d)), the mean ZnO crystallite size increased from 28 nm to 48 nm. At the same time, the aspect ratio of the crystallites increased from 1 to approximately 1.4. The large aspect ratio indicates the formation of elongated, rod-like structures.

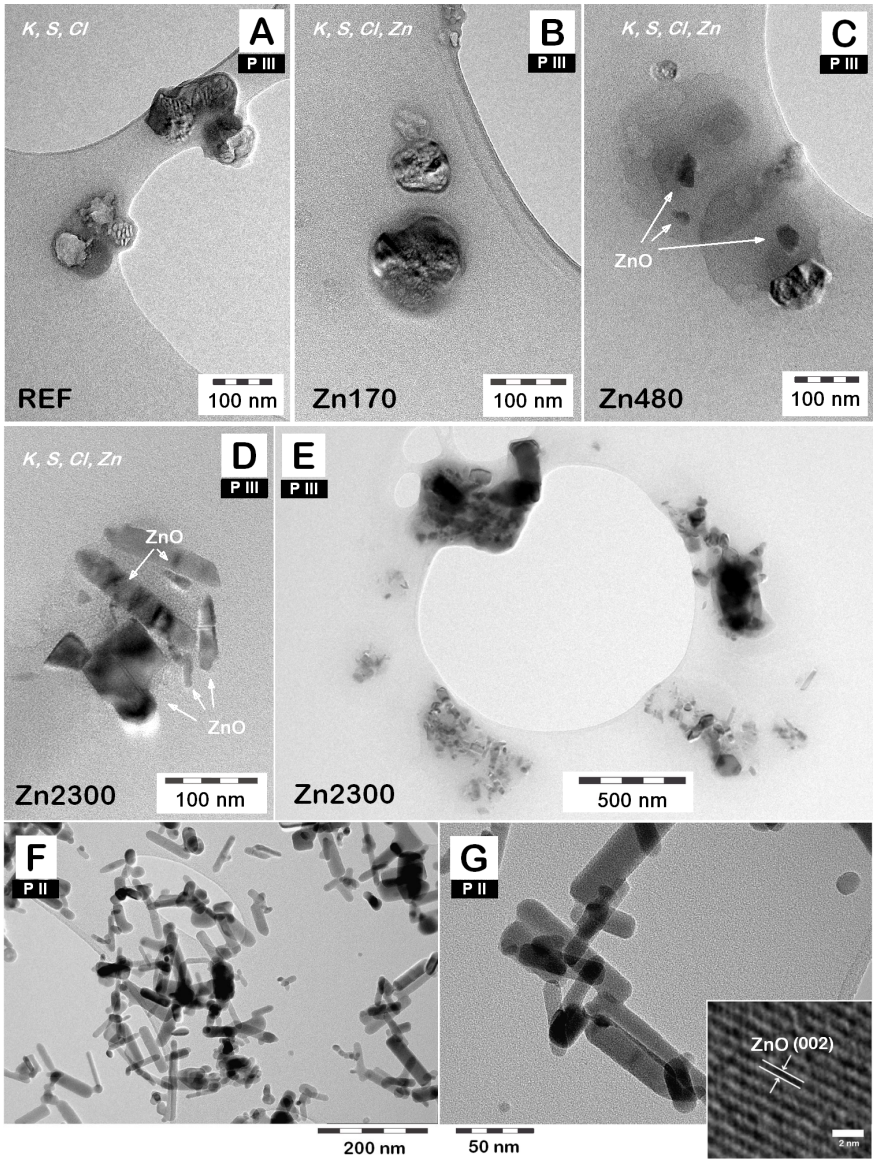

Figure 4.8: TEM micrographs of particles formed in efficient combustion of pellet (A-E, Paper **III***), and in flame synthesis of ZnO (F-G, Paper* **II***). In (A-D) White text in cursive shows the main species generally found in the EDS analysis, as the background components (C, O, Si and Cu) are not included. Zinc was enriched in pellet combustion PM, so that the crystalline ZnO nuclei were seen in zinc rich samples Zn480 and Zn2300 (C-E). Combustion of zinc rich pellet results in the same crystalline phase of ZnO as in flame synthesis (F-G).*

At high Zn concentrations in the fuel, the rod-like crystal shape (Fig. 4.8(d-e)) was the most abundant. It is similar to the thermodynamically stable crystal habit of the wurtzite phase ZnO [6, 75]. More variations in the shapes and sizes of the ZnO particles (Fig. 4.8(d)) was generated in nonuniform growth conditions, which are typical of flame processes with high reaction kinetics and large temperature gradients [67].

At low Zn concentrations in the fuel, the resulting particle appearance (Fig. 4.8(a-c)) and composition were dominated by other condensing species. Small and nearly spherical ZnO nuclei at Zn480 (Fig. 4.8(c)) were observed. Thermodynamic calculations showed that the gas-to-solid transformation temperature of ZnO was decreased both at low fuel concentration of Zn and in reducing atmospheres, which gave less time for single crystal growth.

The crystalline phase of ZnO was not found in PM_1 of pure pellet combustion (Fig. 4.8(a)), although in the ICP-MS analysis Zn was detected. In this case, the primary nucleation of alkali species was the dominant step for fine ash formation and growth because the ZnO seeds were less abundant due to the low concentration, which is in agreement with the previous studies [56]. The lowest concentration of added Zn (Zn170) also did not show separate ZnO nuclei that could be observed via TEM (Fig. 4.8(b)).

These results also led to the conclusion that, in ultrafine ash particles with low zinc concentrations, the nuclei may be receptive to chemical alterations, possibly via surface and volume reactions enhanced by the catalytic activity of ZnO. Moreover, the metastable phases of zinc species may exist if the reaction kinetics at the time of the formation of particles is too fast to enable stable crystal formation. The alterations may lead to very different electrodynamic, adsorptive, reflective and rheological properties of the particles, which may affect the overall toxicities of the particles.

4.4 FORMATION OF ENGINEERED NANOPARTICLES

Flame spray synthesis was used in Paper **II** to produce nanoparticles with known composition to act as model species for wood PM toxicity. This process was an example of fast reaction kinetics where the temperature is high, the time scales are short relative to the quench times, and the supersaturation ratios are high. Therefore, a reaction flow tube with the temperature fixed at 1000 °C was used after the flame, to allow time for the chemical reaction rate-limited processes, e.g., sulfation.

First, pure wurtzite phase ZnO single crystal nanorods (Fig. 4.8(f-g)) were manufactured in Paper **II**. The ZnO nanorods studied in Paper **III** (Fig. 4.8(d-e)) had the same phase composition and similar morphological characteristics: the crystallite sizes of the nanorods were 56 nm and 48 nm, and the aspect ratios 2.8 and 1.4 in Papers **II** and **III**, respectively.

Second, nanoparticles (Fig. 4.9) composed of potassium, sulphur, and zinc, were synthesised. The final compositions of the products were mainly K_2SO_4 and K_2CO_3, depending on the precursor. In one process, zinc was added at a very low concentration with potassium and sulphur precursors. The final particles ($K_2SO_4 + Zn$) contained 0.8 % zinc, but the materials analysis revealed no crystalline phase of ZnO in the particles. The discussion in Paper **III** about the chemical speciation of zinc at low mass concentrations of Zn can also be applied to this case.

The mobility diameters of the K_2CO_3 particles were smaller than 40 nm. The small size and high number concentration resulted in agglomeration of the primary particles (Fig. 4.9(a)). Similarly, the mobility diameters of K_2SO_4 and $K_2SO_4 + Zn$ particles (Fig. 4.9(b)) were smaller than 50 nm; however, the appearance of the two samples in the TEM indicated both the semi-volatile nature of the composites and possible growth in the particle phase via agglomeration and coalescence.

The mobility diameters of all composite particles corresponded well with the ultrafine ash particles from efficient combustion of

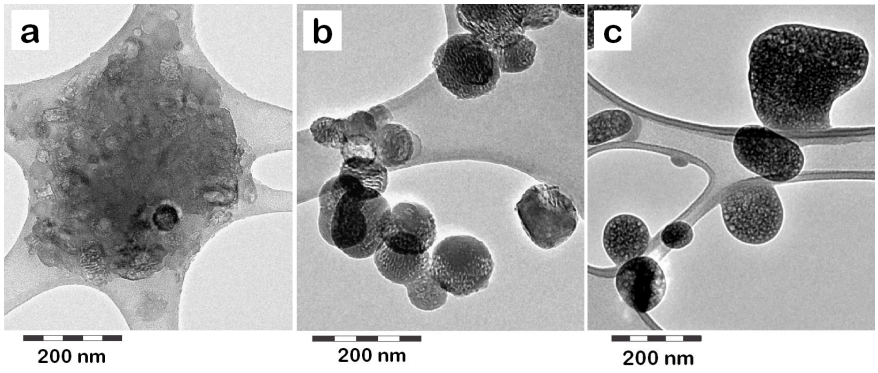

Figure 4.9: TEM images of particles synthesized with the FSP in Paper **II***: (a)* K_2CO_3*, (b),* K_2SO_4 *and (c)* $K_2SO_4 + Zn$ *composite particles.*

wood in Paper **I**. It must be kept in mind that the composite particles were radical simplifications when compared to the complex chemical compositions of the combustion derived fine ash particles studied in Papers **I** and **III**.

The observed similarities in the morphological properties of the particles are important from a toxicological point of view: those materials properties that can be considered causative for toxicological outcomes in engineered nanoparticles could to some extent be applied with the ultrafine particle fraction derived in the combustion processes with high zinc concentrations.

4.5 TOXIC EFFECTS OF THE PARTICLES

In Papers **II** and **IV** the toxicological properties of the combustion and reactor synthesis derived particles were studied. In Paper **II**, the toxicological markers (Table 3.1) were compared at different doses between the PM_1 samples from the flame synthesis (characterised in Paper **II**) and the combustion of wood chips (characterised in Paper **I**). In Paper **IV**, the toxicological markers (Table 3.1) were analysed at different doses for PM_1 from the combustion of zinc-doped and untreated pellets, which were characterised in Paper **III**. In the following discussion, the main results of the toxi-

cology analyses are briefly reviewed.

Acute cytotoxicity: The cytotoxic response of the cells, as determined using the PI-exclusion assay after 24 h of exposure to the particulate matter, are shown in Fig. 4.10 and Fig. 4.11. In Fig. 4.10, the data from the PM samples containing zinc are ordered vertically according to their calculated maximum free zinc ion concentration in the cell culture medium (C_{MFZ}, μg ml^{-1}, right axis).

From the data severe cytotoxic effects occur when the free zinc ion concentration (C_{MFZ}) in the cell medium exceeds 10-30 μg ml^{-1}. Severe cytotoxicity can be expressed as the EC_{50} value, which is the 50 % effective concentration of the maximum. The two sets of data in Papers **II** and **IV** have different control values, and the size of the effect should not be compared in absolute terms. What is notable is that the zinc concentrations needed to evoke severe cytotoxic effects were already reached with a PM sample from untreated wood combustion ("Wood PM, 300" exceeded EC_{50} in Fig. 4.10), and not only in the artificial, pure ZnO samples.

The same data, now including all of the samples and comparing the mass concentrations of the PM, are shown in Fig. 4.11. Samples containing only potassium sulphates or carbonates induced mild cytotoxic effect only with the largest PM dose, compared to the control. The response of the PI-exclusion assay basically shows an increase in the cell membrane permeability, which is indicative of necrotic or late apoptotic cell death. The data suggest severe failures of cellular protective mechanisms at zinc concentrations above 10 μg ml^{-1}.

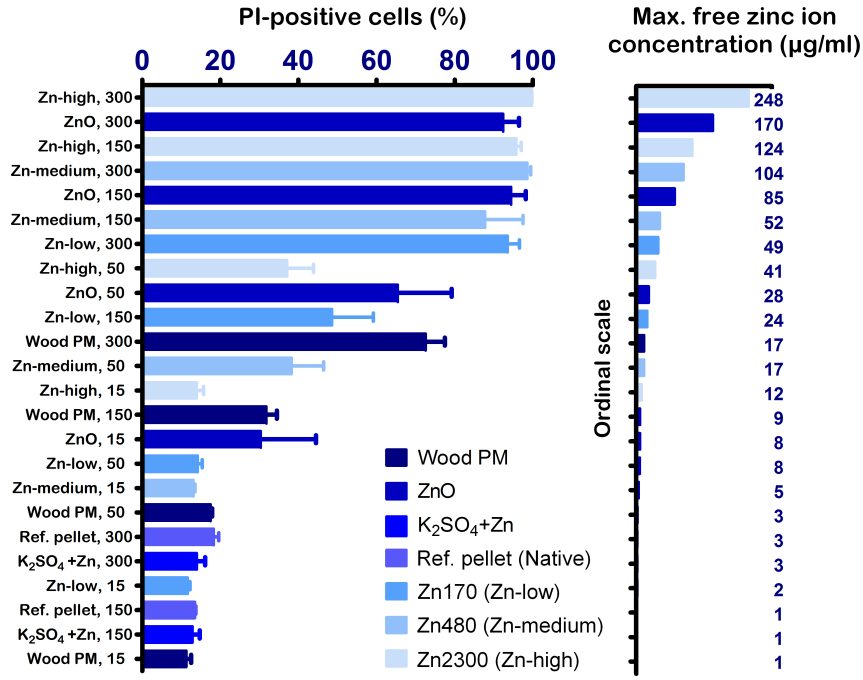

Figure 4.10: Acute cytotoxicity (% of PI-positive cells) of various zinc containing particulate samples, studied in Papers **II-IV**, *ordered by the calculated maximum free zinc ion concentration (μg ml^{-1}) in the cell culture medium. The severe cytotoxic effects (50 % of cells are PI-positive) are observed approximately above free zinc ion concetration of 10-30 μg ml^{-1}. The numbers after sample names present the particulate mass doses (15, 50, 150, and 300 μg ml^{-1}). Sample names correspond to the nomenclature used in Table 3.1.*

Figure 4.11: Acute cytotoxicity (% of PI-positive cells) of various particulate samples, studied in RAW264.7 macrophage cells. Whiskers present the standard error of the mean. The asterisks indicate statistical significance ($p < 0.05$) compared to the blank substrate control (dashed line) analyzed by the nonparametric Kruskal-Wallis test. The letters (a-e in Paper **II**; *a-d in Paper* **IV**) *indicate a statistically significantly larger ($p < 0.05$) response compared to other PM doses, based on ANOVA and Tukey's test. On the top scale, the compared samples are the synthesized composite nanoparticles and PM_1 from wood combustion (Paper* **II**). *On the bottom scale, pellet PM samples with increasing loading of zinc (Papers* **III** *and* **IV**) *are compared. Sample names correspond to the nomenclature used in Table 3.1 and in Papers* **II** *and* **IV**.

Cell cycle and generation of ROS: In addition to cytotoxicity, analyses of the generation of ROS and cell cycle arrest support the role of Zn in the toxicity of the PM samples. First, wood PM (Paper **II**) and all of the zinc-rich samples (Papers **II** and **IV**) caused a significant generation of ROS in cells. The ZnO nanoparticles and Zn^{2+} are known to be able to trigger extensive oxidative stress in a variety of cell lines [7]. The generation of ROS is indicative of a broad range of adverse outcomes in cells, which are called oxidative stress [87,91]. The Zn^{2+} does not produce ROS, so the ROS must have an endogenous cellular origin, e.g., produced by mitochondria [1]. Second, accumulation of the macrophage cells during the S-G_2/M cell cycle phase, indicating cell cycle arrest in G_2 phase, was observed with increasing Zn concentration, which is in line with the previous results [118]. Moreover, an increased number of apoptotic cells was observed in cultures exposed to the wood combustion samples, i.e., wood PM (Paper **II**) and the reference pellet (Paper **IV**), at high particle mass concentrations. The amount of organic carbon and related PAHs were equally low for the both PM samples, so that they were not assumed to be related to the oberved toxicological effects. However, the possible effects of other species, e.g., chromium, and the coupled effects between species may be important and cannot be ruled out.

Inflammation and genotoxicity: The generation of inflammatory mediators TNF-α (Papers **II** and **IV**) and MIP-2 (Paper **IV**) in the mouse macrophage cell line were not directly connected to either the concentration of zinc in the PM samples or the mass dose. These two markers were determined outside the cells from the cell culture medium and can be affected by the decreased metabolic activity of the cells. Many different reasons for the decreased metabolic activity can be found, for example, the disturbed cell cycle, broken cell membrane, and necrosis or apoptosis. Refinement of the issue could be obtained by using multiple time points to see the evolution of the inflammation. In contrast, the high inflammation potential of PM could in some instances be linked to the incompleteness of the combustion [119], which was not studied in these papers.

The genotoxicity study in Paper **IV** was also affected by the massive cytotoxicity, which reduced the number of analysable samples. However, it was observed that the reference pellet PM_1 induced a dose-dependent increase in Olive tail moment (OTM), with a statistically significant effect at the two highest doses. The effect could be a secondary occurence to the inflammation or a response to the increased ROS production. The OTM marker was not used to compare the particles examined in Paper **II**.

Non-responsive PM: The alkali species alone, which were synthesised in Paper **II**, did not cause cytotoxicity, cell cycle arrest, ROS generation, or an inflammation response in the studied mouse macrophage cell model. These observations underline the role of trace metals, especially zinc enrichment, in the PM-induced toxic effects.

Although the Zn^{2+} ion concentration was connected to the toxic effects in this study, it has been shown *in vitro* that ZnO particles may also induce toxic reactions without significant free ion release rate into the medium [92, 120, 121]. The proposed mechanism is the internalisation of ZnO nanoparticles into cells prior to dissolution, which is also a possible pathway for the PM toxicity in this study. The cell culture medium with various dissolved salts and proteins also plays a key role in the dissolution and distribution of all species, which implies that more attention should be given to the particle dissolution behaviour in future studies.

In addition, as stated previously, it is most likely that the chemical and physical state of Zn (molecular binding, crystal structure, size, and spatial distribution) in the PM varies between the fuels, sources, and even within the particulate emission from a single source. These factors most likely affect the ZnO dissolution and internalisation rates and, consequently, the toxic mechanisms in the biological matrix. Therefore, the PM materials properties, especially the metastable phases of the species at the nanosized level, should be studied further. A more thorough study of the toxicological effects of biomass combustion generated fine particles, including those studied in this thesis (Papers **II** and **IV**), was recently

published as a doctoral dissertation. For more information, please see reference [1].

5 Author's contribution

The publications selected in this dissertation are original research papers.

The author is responsible for the manuscript writing, electron microscopy and data analyses, and thermodynamical equilibrium calculations in Paper **I** under the supervision of Prof. J. Jokiniemi and Ph.D. J. Tissari. The combustion experiments were designed by Ph.D. (Tech.) O. Sippula and Ph.D. J. Tissari, and conducted as part of the Biohealth project in Fine Particle and Aerosol Technology Laboratory. The aerosol measurement and bulk chemical analysis data for the manuscript were provided by M.Sc. J. Leskinen, M.Sc. T. Kaivosoja and M.Sc. A. Virén.

The author is responsible for the manuscript writing and data analysis in Paper **II**. M.Sc. O. Uski conducted the toxicological analyses under supervision of Prof. Maija-Riitta Hirvonen, and wrote the main toxicological result analysis in the manuscript. The particle synthesis experiments were designed and conducted by M.Sc. T. Karhunen under supervision of Prof. J. Jokiniemi and Ph.D. A. Lähde. M.Sc. T. Karhunen was also responsible for the XRD analysis in the paper.

Papers **III** and **IV** are parallel studies on the same measurement campaign, conducted in the University of Eastern Finland. Ph.D. J. Tissari wrote the manuscript of Paper **III**. M.Sc. O. Uski conducted the toxicological analyses under supervision of Prof. Maija-Riitta Hirvonen, and wrote the manuscript of Paper **IV**. The author was responsible for electron microscopy analyses and writing the materials analysis parts on the manuscripts and the supplementaries.

Papers **II** and **IV** were also included in Oskari Uski's doctoral thesis [1] which concentrated on the toxic effects of the emissions.

6 Conclusions

The primary objective of this study was to gain a better understanding of the connections between the chemical speciation in combustion related gas-to-particle formation processes and the particle morphological features, such as size, shape, surface structure and solid phase. The observations were discussed with respect to the particle-induced toxicological responses in mouse macrophage cells, especially those related to zinc enrichment in ultrafine particles.

The conditions during the particle formation and growth affected the morphological features that were observable by TEM. The study showed the importance of organic species on the surface structure and shape of freshly emitted particles, though only the low-volatility fraction of the organics could be observed. In addition, the observations of the mixing state of the combustion particles indicated that in incomplete combustion, the ultrafine ash fraction crosses into the accumulation mode, which may reduce exposure to these components via inhalation. Under optimal combustion conditions, mixing does not occur, and the particles remain in the ultrafine mode.

Moreover, the ZnO nuclei were identified inside the ash fraction of untreated wood PM; however, their abundance was dependent on the concentration of Zn in the fuel. In addition, the influence of Zn concentration in the fuel on the morphology of PM was demonstrated. The equilibrium structure of hexagonal ZnO could be recognised at high fuel concentrations, which can be assessed from waste incineration and nanomaterial engineering. At low concentrations of Zn in the fuel, the size of the crystalline ZnO decreased, and the phase state of the Zn could no longer be identified. Diffraction contrast methods were used to identify the nanocrystalline phases of ZnO in the ultrafine mode whenever they could not be assessed using regular analytical methods. The possibility

of physical or chemical transformations of ZnO in the presence of suitable reactants was speculated.

While engineered nanoparticles and the particulate mass from biomass combustion differ significantly, in many instances these two materials have a close resemblance in physical appearance and chemical composition. In particular, the current study shows similar features between nanoengineered ZnO particle formation and ZnO transfer from biofuel to the fresh emission PM_1. In the study, similar toxicological responses were evoked by both materials, primarily due to the enrichment of zinc. The potassium sulphates and carbonates engineered and used as model particles for alkali species in ambient PM, did not evoke toxicological responses.

In summary, the evaluation of the environmental and adverse health effects based on average particle property values can be highly misleading due to the heterogeneity of the emissions. The morphological features have consequences on the fate of these particles in, for example, lung epithelium, as their solubility and electrical properties strongly depend on their solid phase. The findings agree with the results of the previous studies, which indicate that equivalent masses of particles from near-complete wood combustion can be more potent inducers of oxidative stress than those emitted from more incomplete combustion processes. The current study indicates that the properties of the biomass fuel are directly related to the toxicological properties of the emission, which may help with the selection of fuel. Paying attention to the volatile transition metal content in woody fuels could be the most direct way to avoid potential problems.

The connections between the morphological features and toxicity of fine PM still have open questions. Further studies of the metastable phases of transition metals and their behaviour in the presence of alkali salts, are needed. Using the aerosol methods, more versatile model particles could be developed by combining both inorganic and organic materials as references for the toxicity of the PM. Moreover, the study of the behaviour of multicomposite particles in biological solutions would help increase understanding

of the various toxicity pathways induced by PM. There are methods for assessing the structure of nanocrystalline particles, such as fluctuation electron microscopy, which are more useful for metastable phases of materials than the analysis methods used in this thesis. Finally, it would be interesting to develop more advanced methods for sampling in high temperature environments, e.g., in flames, to clarify the early stages of the particle formation.

Bibliography

[1] O. Uski, *Toxicological effects of fine particles from small-scale biomass combustion*, PhD thesis (University of Eastern Finland, 2014).

[2] R. Silva, J. West, Y. Zhang, S. Anenberg, J.-F. Lamarque, D. Shindell, W. Collins, S. Dalsoren, G. Faluvegi, G. Folberth, L. Horowitz, T. Nagashima, V. Naik, S. Rumbold, R. Skeie, K. Sudo, T. Takemura, D. Bergmann, P. Cameron-Smith, I. Cionni, R. Doherty, V. Eyring, B. Josse, I. MacKenzie, D. Plummer, M. Righi, D. Stevenson, S. Strode, S. Szopa, and G. Zeng, "Global premature mortality due to anthropogenic outdoor air pollution and the contribution of past climate change," *Environmental Research Letters* **8,** 034005 (2013).

[3] S. Saarikoski, M. Sillanpää, K. Saarnio, R. Hillamo, A. Pennanen, and R. Salonen, "Impact of biomass combustion on urban fine particulate matter in Central and Northern Europe," *Water, Air, & Soil Pollution* **191,** 265–277 (2008).

[4] European Commission, "Proposal for Directive of the European Parliament and of the Council on the promotion of use of renewable energy sources," (2008), COD 2008/0016.

[5] P. J. Borm, D. Robbins, S. Haubold, T. Kuhlbusch, H. Fissan, K. Donaldson, R. Schins, V. Stone, W. Kreyling, J. Lademann, J. Krutmann, D. Warheit, and E. Oberdorster, "The potential risks of nanomaterials: a review carried out for ECETOC," *Particle and fibre toxicology* **3** (2006).

[6] Z. L. Wang, "Zinc oxide nanostructures: growth, properties and applications," *Journal of Physics: Condensed Matter* **16,** R829–R858 (2004).

[7] W. Wu, P. Bromberg, and J. Samet, "Zinc ions as effectors of environmental oxidative lung injury.," *Free radical biology & medicine* **65,** 57–69 (2013).

[8] P. E. Schwarze, J. Ovrevik, M. Lag, M. Refsnes, P. Nafstad, R. B. Hetland, and E. Dybing, "Particulate matter properties and health effects: consistency of epidemiological and toxicological studies," *Human & Experimental Toxicology* **25,** 559–579 (2006).

[9] P. Gilmour, D. Brown, P. Beswick, E. Benton, W. MacNee, and K. Donaldson, "Surface free radical activity of PM10 and ultrafine titanium diozide: a unifying factor in their toxicity?," *Annals of Occupational Hygiene* 32-38 (1997).

[10] F. Cassee, M.-E. Héroux, M. Gerlofs-Nijland, and F. Kelly, "Particulate matter beyond mass: recent health evidence on the role of fractions, chemical constituents and sources of emission," *Inhalation Toxicology* **25,** 802–812 (2013).

[11] M. S. Happo, O. Uski, P. I. Jalava, J. Kelz, T. Brunner, P. Hakulinen, J. Mäki-Paakkanen, V.-M. Kosma, J. Jokiniemi, I. Obernberger, , and M.-R. Hirvonen, "Pulmonary inflammation and tissue damage in the mouse lung after exposure to PM samples from biomass heating appliances of old and modern technologies," *Sci Total Environ* **443,** 256–266 (2013).

[12] O. J. Uski, M. S. Happo, P. I. Jalava, T. Brunner, J. Kelz, I. Obernberger, J. Jokiniemi, and M.-R. Hirvonen, "Acute systemic and lung inflammation in C57Bl/6J mice after intratracheal aspiration of particulate matter from small-scale biomass combustion appliances based on old and modern technologies," *Inhalation Toxicology* **24,** 952–965 (2012).

[13] C. Senior and R. Flagan, "Ash vaporization and condensation during combustion of a suspended coal particle," *Aerosol Science and Technology* **1,** 371–383 (1982).

[14] M. Jöller, T. Brunner, I. Obernberger, and I. Letofsky-Pabst, "Investigation of formation pathways of aerosol particles formed during fixed bed combustion of woody biomass fuels," *Preprints of Papers-American Chemical Society, Division of Fuel Chemistry* **49,** 85–86 (2004).

[15] A. Fernandez, S. B. Davis, J. O. Wendt, R. Cenni, S. R. Young, and M. L. Witten, "Particulate emission from biomass combustion," *Nature* **409,** 998–998 (2001).

[16] P. Sielicki, H. Janik, A. Guzman, and J. Namieśnik, "The progress in electron microscopy studies of particulate matters to be used as a standard monitoring method for air dust pollution," *Critical Reviews in Analytical Chemistry* **41,** 314–334 (2011).

[17] W. Hinds, *Aerosol Technology: Properties, behaviour and measurement of airborne particles*, second ed. (John Wiley & Sons Inc., New Jersey, USA, 1992).

[18] M. Kanakidou, J. H. Seinfeld, S. N. Pandis, I. Barnes, F. J. Dentener, M. C. Facchini, R. Van Dingenen, B. Ervens, A. Nenes, C. J. Nielsen, E. Swietlicki, J. P. Putaud, Y. Balkanski, S. Fuzzi, J. Horth, G. K. Moortgat, R. Winterhalter, C. E. L. Myhre, K. Tsigaridis, E. Vignati, E. G. Stephanou, and J. Wilson, "Organic aerosol and global climate modelling: a review," *Atmospheric Chemistry and Physics* **5,** 1053–1123 (2005).

[19] L. Mädler and S. Friedlander, "Transport of nanoparticles in gases: overview and recent advances," *Aerosol and Air Quality Research* **7,** 304–342 (2007).

[20] J. Araujo and A. Nel, "Particulate matter and atherosclerosis: role of particle size, composition and oxidative stress," *Particle and Fibre Toxicology* **6,** 24 (2009).

[21] V. Vakkari, V.-M. Kerminen, J. P. Beukes, P. Tiitta, P. G. van Zyl, M. Josipovic, A. D. Venter, K. Jaars, D. R. Worsnop, M. Kulmala, and L. Laakso, "Rapid changes in biomass burning aerosols by atmospheric oxidation," *Geophysical Research Letters* **41,** 2644–2651 (2014).

[22] A. Ghio, J. Soukup, M. Case, L. Dailey, J. Richards, J. Berntsen, R. Devlin, S. Stone, and A. Rappold, "Exposure to wood smoke particles produces inflammation in healthy volunteers.," *Occupational and environmental medicine* **69,** 170–175 (2012).

[23] J. Seinfeld and S. Pandis, *Atmospheric Chemistry and Physics: From air pollution to climate change*, second ed. (John Wiley & Sons Inc., New Jersey, USA, 2006).

[24] K. R. Spurny, ed., *Aerosol chemical processes in the environment* (CRC Press, 2000).

[25] H. Kassman, L. Bäfver, and L.-E. Åmand, "The importance of SO2 and SO3 for sulphation of gaseous KCl: An experimental investigation in a biomass fired CFB boiler," *Combustion and Flame* **157,** 1649 – 1657 (2010).

[26] C. Bale, P. Chartrand, S. Degterov, G. Eriksson, K. Hack, K. Mahfoud, J. Melancon, A. Pelton, and S. Petersen, "Factsage thermochemical software and databases," *Calphad* **26,** 189–228 (2002).

[27] N. Donahue, A. Robinson, and S. Pandis, "Atmospheric organic particulate matter: From smoke to secondary organic aerosol," *Atmospheric Environment* **43** (2009).

[28] O. Sippula, T. Koponen, and J. Jokiniemi, "Behavior of Alkali Metal Aerosol in a High-Temperature Porous Tube Sampling Probe," *Aerosol Science and Technology* **46,** 1151–1162 (2012).

[29] J. A. Rodriguez, T. Jirsak, S. Chaturvedi, and J. Dvorak, "Chemistry of SO2 and NO2 on ZnO(0001)-Zn and ZnO powders: changes in reactivity with surface structure and composition," *Journal of Molecular Catalysis A: Chemical* **167,** 47–57 (2001).

[30] R. Ma, C. Levard, F. M. Michel, G. E. Brown, and G. V. Lowry, "Sulfidation mechanism for zinc oxide nanoparticles and the effect of sulfidation on their solubility.," *Environmental science & technology* **47,** 2527–2534 (2013).

[31] K. Lehtinen, "A Note on the Growth of Primary Particles in Agglomerate Structures by Coalescence," *Journal of Colloid and Interface Science* **182** (1996).

[32] R. Givehchi and Z. Tan, "An Overview of Airborne Nanoparticle Filtration and Thermal Rebound Theory," *Aerosol and Air Quality Research* **14,** 45–63 (2014).

[33] M. Lippmann, D. Yeates, and R. Albert, "Deposition, retention, and clearance of inhaled particles," *Br. J. Ind. Med.* **37,** 337–362 (1980).

[34] M. Smooke, C. McEnally, L. Pfefferle, and R. Hall, "Computational and experimental study of soot formation in a coflow, laminar diffusion flame," *Combustion and Flame* **117,** 117–139 (1999).

[35] E. Fitzpatrick, A. Ross, J. Bates, G. Andrews, J. Jones, H. Phylaktou, M. Pourkashanian, and A. Williams, "Emission of Oxygenated Species from the Combustion of Pine Wood and its Relation to Soot Formation," *Process Safety and Environmental Protection* **85,** 430 – 440 (2007).

[36] H. Lamberg, O. Sippula, J. Tissari, and J. Jokiniemi, "Effect of air-staging and load on fine particle and gaseous emissions from small-scale pellet boiler," *Energy & Fuels* **25,** 4952–4960 (2011).

[37] L. Mädler, H. Kammler, R. Mueller, and S. Pratsinis, "Controlled synthesis of nanostructured particles by flame spray pyrolysis," *Journal of Aerosol Science* **33,** 369–389 (2002).

[38] R. J. Yokelson, I. R. Burling, J. B. Gilman, C. Warneke, C. E. Stockwell, J. de Gouw, S. K. Akagi, S. P. Urbanski, P. . Veres, J. M. Roberts,

W. C. Kuster, J. Reardon, D. W. T. Griffith, T. J. Johnson, S. Hosseini, J. W. Miller, D. R. C. III, H. Jung, and D. R. Weise, "Coupling field and laboratory measurements to estimate the emission factors of identified and unidentified trace gases for prescribed fires," *Atmospheric Chemistry and Physics* **13,** 89–116 (2013).

[39] S. van Loo and J. Koppejan, eds., *The handbook of biomass combustion and co-firing* (Earthscan, 2008).

[40] E. M. Fitzpatrick, J. M. Jones, M. Pourkashanian, A. B. Ross, A. Williams, and K. D. Bartle, "Mechanistic aspects of soot formation from the combustion of pine wood," *Energy & Fuels* **22,** 3771–3778 (2008).

[41] A. Williams, J. Jones, L. Ma, and M. Pourkashanian, "Pollutants from the combustion of solid biomass fuels," (2012).

[42] M. Hays and R. Vander Wal, "Heterogeneous soot nanostructure in atmospheric and combustion source aerosols," *Energy and Fuels* **21,** 801–811 (2007).

[43] H. Richter and J. Howard, "Formation of polycyclic aromatic hydrocarbons and their growth to soot – a review of chemical reaction pathways," *Progress in Energy and Combustion Science* **26,** 565 – 608 (2000).

[44] H. Chen and R. Dobbins, "Crystallogenesis of particles formed in hydrocarbon combustion," *Combustion Science and Technology* **159,** 109–128 (2000).

[45] R. Vander Wal, "Soot precursor carbonization: Visualization using LIF and LII and comparison using bright and dark field TEM," *Combustion and Flame* **112,** 607–616 (1998).

[46] R. Vander Wal and C. Mueller, "Initial investigation of effects of fuel oxygenation on nanostructure of soot from a direct-injection diesel engine," *Energy & Fuels* 2364-2369 (2006).

[47] T. Ishiguro, Y. Takatori, and K. Akihama, "Microstructure of diesel soot particles probed by electron microscopy: first observation of inner core and outer shell," *Combustion and Flame* **108,** 231–234 (1997).

[48] K. Nuutinen, J. Jokiniemi, O. Sippula, H. Lamberg, J. Sutinen, P. Horttanainen, and J. Tissari, "Effect of air staging on fine particle, dust and gaseous emissions from masonry heaters," *Biomass and Bioenergy* **67,** 167–178 (2014).

[49] A. F. Khalizov, R. Zhang, D. Zhang, H. Xue, J. Pagels, and P. H. McMurry, "Formation of highly hygroscopic soot aerosols upon internal mixing with sulfuric acid vapor," *Journal of Geophysical Research: Atmospheres* **114,** D05208 (2009).

[50] P. Tiitta, V. Vakkari, P. Croteau, J. Beukes, P. Zyl, M. Josipovic, A. Venter, K. Jaars, J. Pienaar, N. Ng, M. Canagaratna, J. jayne, V.-M. Kerminen, H. Kokkola, M. Kulmala, A. Laaksonen, D. Worsnop, and L. Laakso, "Chemical composition, main sources and temporal variability of PM₁ aerosols in southern African grassland," *Atmospheric Chemistry and Physics* **14,** 1909–1927 (2014).

[51] K. Hytönen, P. Yli-Pirilä, J. Tissari, A. Gröhn, I. Riipinen, K. Lehtinen, and J. Jokiniemi, "Gas-particle distribution of PAHs in wood combustion emission determined with annular denuders, filter, and polyurethane foam adsorbent," *Aerosol Science and Technology* **43,** 442–454 (2009).

[52] O. Sippula, K. Hytönen, J. Tissari, T. Raunemaa, and J. Jokiniemi, "Effect of Wood Fuel on the Emissions from a Top-Feed Pellet Stove," *Energy & Fuels* **21,** 1151–1160 (2007).

[53] O. Sippula, T. Lind, and J. Jokiniemi, "Effects of chlorine and sulphur on particle formation in wood combustion performed in a laboratory scale reactor," *Fuel* **87,** 2425–2436 (2008).

[54] L. Åmand, B. Leckner, D. Eskilsson, and C. Tullin, "Ash Deposition on Heat Transfer Tubes during Combustion of Demolition Wood," *Energy & Fuels* **20,** 1001–1007 (2006).

[55] M. Wornat, R. Hurt, N. Yang, and T. Headly, "Structural and Compositional Transformation of Biomass Chars during Combustion," *Combustion and Flame* **100,** 131–143 (1995).

[56] M. Jöller, T. Brunner, and I. Obernberger, "Modeling of aerosol formation during biomass combustion for various furnace and boiler types," *Fuel Processing Technology* **88,** 1136 – 1147 (2007), Impacts of Fuel Quality on Power Production.

[57] O. Sippula, *Fine particle formation and emissions in biomass combustion*, PhD thesis (University of Eastern Finland, 2010).

[58] M. Strand, *Particle formation and emission in moving grate boilers operating on woody biofuels*, PhD thesis (Växjö University, 2004).

[59] M. Jöller, T. Brunner, and I. Obernberger, "Modeling of aerosol formation during biomass combustion in grate furnaces and comparison with measurements," *Energy and Fuels* **19,** 311–323 (2005).

[60] H. Wiinikka, R. Gebart, C. Boman, D. Boström, and M. Öhman, "Influence of fuel ash composition on high temperature aerosol formation in fixed bed combustion of woody biomass pellets," *Fuel* **86,** 181 – 193 (2007).

[61] O. Sippula, J. Hokkinen, H. Puustinen, P. Yli-Pirilä, and J. Jokiniemi, "Comparison of particle emissions from small heavy fuel oil and wood-fired boilers," *Atmospheric Environment* **43,** 4855–4864 (2009).

[62] L. Tumolva, J.-Y. Park, J.-S. Kim, A. Miller, J. Chow, J. Watson, and K. Park, "Morphological and elemental classification of freshly emitted soot particles and atmospheric ultrafine particles using the TEM/EDS," *Aerosol Science and Technology* **44,** 202–215 (2010).

[63] A. Nel, T. Xia, L. Mädler, and N. Li, "Toxic potential of materials at the nanolevel," *Science (New York, N.Y.)* **311,** 622–627 (2006).

[64] M. Hosokawa, K. Nogi, M. Naito, and T. Yokoyama, eds., *Nanoparticle technology handbook* (Elsevier, 2007).

[65] G. Oberdörster, E. Oberdörster, and J. Oberdörster, "Nanotoxicology: an emerging discipline evolving from studies of ultrafine particles," *Environmental Health Perspectives* **113,** 823–830 (2005).

[66] J. Fang, H. Nakamura, and H. Maeda, "The EPR effect: Unique features of tumor blood vessels for drug delivery, factors involved, and limitations and augmentation of the effect," *Advanced Drug Delivery Reviews* **63,** 136–151 (2011).

[67] S. Pratsinis, "Aerosol based technologies in nanoscale manufacturing: from functional materials to devices through core chemical engineering," *AIChE Journal* **56,** 3028–3035 (2010).

[68] T. Torvela, A. Lähde, J. Mönkäre, J. Riikonen, K. Lehtinen, K. Järvinen, V.-P. Lehto, J. Jokiniemi, and J. Joutsensaari, "Low-temperature aerosol flow reactor method for preparation of surface stabilized pharmaceutical nanocarriers," *Journal of Aerosol Science* **42,** 645–656 (2011).

[69] S. Yu, G. Wu, X. Gu, J. Wang, Y. Wang, H. Gao, and M. Jianbiao, "Magnetic and pH-sensitive nanoparticles for antitumor drug delivery," *Colloids and Surfaces B: Biointerfaces* **103,** 15–22 (2013).

[70] N. Ashcroft and N. Mermin, *Solid state physics* (Harcourt College publishers, US, 1976).

[71] D. Williams and C. Carter, *Transmission Electron Microscopy*, 2 ed. (Springer, 2009).

[72] J. Joutsensaari, P. Ahonen, and E. Kauppinen, "Aerosol synthesis of fullerene nanocrystals in controlled flow reactor conditions," *Journal of Nanoparticle Research* **2,** 53–74 (2000).

[73] R. Zallen, *The Physics of amorphous solids* (John Wiley & Sons, 1983).

[74] C. Hammond, *The basics of crystallography and diffraction*, 3 ed. (Oxford University Press, 2009).

[75] C. Ye, X. Fang, Y. Hao, X. Teng, and L. Zhang, "Zinc oxide nanostructures: morphology derivation and evolution.," *The journal of physical chemistry. B* **109,** 19758–19765 (2005).

[76] A. Navrotsky, "Energetics of nanoparticle oxides: interplay between surface energy and polymorphism," *Geochemical Transactions* **4,** 34–37 (2003).

[77] Y.-N. Chang, M. Zhang, L. Xia, J. Zhang, and G. Xing, "The toxic effects and mechanisms of CuO and ZnO nanoparticles," *Materials* **5,** 2850–2871 (2012).

[78] F. Jones, H. Tran, D. Lindberg, L. Zhao, and M. Hupa, "Thermal Stability of Zinc Compounds," *Energy & Fuels* **27,** 5663–5669 (2013).

[79] S. Walia, S. Balendhran, H. Nili, S. Zhuiykov, G. Rosengarten, Q. H. Wang, M. Bhaskaran, S. Sriram, M. S. Strano, and K. Kalantar-zadeh, "Transition metal oxides – Thermoelectric properties," *Progress in Materials Science* **58,** 1443 – 1489 (2013).

[80] C. Wöll, "The chemistry and physics of zinc oxide surfaces," *Progress in Surface Science* **82** (2007).

[81] K. Momma and F. Izumi, "VESTA 3 for three-dimensional visualization of crystal, volumetric and morphology data," *Journal of Applied Crystallography* **44,** 1272–1276 (2011).

[82] S. Chaturvedi, J. A. Rodriguez, T. Jirsak, and J. Hrbek, "Surface Chemistry of SO2on Zn and ZnO: Photoemission and Molecular Orbital Studies," *The Journal of Physical Chemistry B* **102,** 7033–7043 (1998).

[83] A. W. Grant, A. Jamieson, and C. T. Campbell, "Adsorption of chlorine on ZnO(0001)–Zn and coadsorption with HCOOH," *Surface Science* **458,** 71–79 (2000).

[84] F. Jones, D. Bankiewicz, and M. Hupa, "Occurrence and sources of zinc in fuels," *Fuel* **117,** 763–775 (2014).

[85] A. Nemmar, J. A. Holme, I. Rosas, P. E. Schwarze, and E. Alfaro-Moreno, "Recent advances in particulate matter and nanoparticle toxicology: a review of the in vivo and in vitro studies," *BioMed Research International* (2013), ID:279371.

[86] B. Brunekreef and S. Holgate, "Air pollution and health," *Lancet* **360,** 1233–1242 (2002).

[87] T. Xia, M. Kovochich, J. Brant, M. Hotze, J. Sempf, T. Oberley, C. Sioutas, J. I. Yeh, M. R. Wiesner, and A. E. Nel, "Comparison of the abilities of ambient and manufactured nanoparticles to induce cellular toxicity according to an oxidative stress paradigm.," *Nano Lett.* **6,** 1794–1807 (2006).

[88] A. Yang, A. Jedynska, B. Hellack, I. Kooter, G. Hoek, B. Brunekreef, T. A. Kuhlbusch, F. R. Cassee, and N. A. Janssen, "Measurement of the oxidative potential of PM2.5 and its constituents: The effect of extraction solvent and filter type," *Atmospheric Environment* **83,** 35 – 42 (2014).

[89] A. J. Ghio, "Biological effects of Utah Valley ambient air particles in humans: a review," *Journal of Aerosol Medicine* **17,** 157–164 (2004).

[90] T. Buerki-Thurnherr, L. Xiao, L. Diener, O. Arslan, C. Hirsch, X. Maeder-Althaus, K. Grieder, B. Wampfler, S. Mathur, P. Wick, and H. F. Krug, "In vitro mechanistic study towards a better understanding of ZnO nanoparticle toxicity," *Nanotoxicology* **7,** 402–416 (2013).

[91] S. Pokhrel, A. Nel, and L. Mädler, "Custom-Designed Nanomaterial Libraries for Testing Metal Oxide Toxicity.," *Accounts of chemical research* **46,** 632–641 (2013).

[92] T. Xia, M. Kovochich, M. Liong, L. Mädler, B. Gilbert, H. Shi, J. Yeh, J. Zink, and A. Nel, "Comparison of the mechanism of toxicity of zinc oxide and cerium oxide nanoparticles based on dissolution and oxidative stress properties.," *ACS nano* **2,** 2121–2134 (2008).

[93] S. J. Park, Y. C. Park, S. W. Lee, M. S. Jeong, K. N. Yu, H. Jung, J. K. Lee, J. S. Kim, and M. H. Cho, "Comparing the toxic mechanism of synthesized zinc oxide nanomaterials by physicochemical characterization and reactive oxygen species properties.," *Toxicology letters* **207,** 197–203 (2011).

[94] W. Lin, Y. Xu, C. Huang, Y. Ma, K. B. Shannon, D. Chen, and Y. Huang, "Toxicity of nano-and micro-sized ZnO particles in human lung epithelial cells," *Journal of Nanoparticle Research* **11,** 25–39 (2009).

[95] I. Hsiao and Y. Huang, "Titanium oxide shell coatings decrease the cytotoxicity of ZnO nanoparticles.," *Chemical research in toxicology* **24,** 303–313 (2011).

[96] G. Sotiriou, C. Watson, K. Murdaugh, T. Darrah, G. Pyrgiotakis, A. Elder, J. Brain, and P. Demokritou, "Engineering safer-by-design silica-coated ZnO nanorods with reduced DNA damage potential," *Environmental Science: Nano* **1,** 144–153 (2014).

[97] M. Luo, C. Shen, B. N. Feltis, L. L. Martin, A. E. Hughes, P. F. Wright, and T. W. Turney, "Reducing ZnO nanoparticle cytotoxicity by surface modification.," *Nanoscale* (2014).

[98] P. Toth, A. Palotas, E. Eddings, R. Whitaker, and J. Lighty, "A novel framework for the quantitative analysis of high resolution transmission electron micrographs of soot I. Improved measurement of interlayer spacing," *Combustion and Flame* **160,** 909–919 (2013).

[99] W. Li and L. Shao, "Transmission electron microscopy study of aerosol particles from the brown hazes in northern China," *Journal of geophysical research* **114** (2009).

[100] J. Tissari, K. Hytönen, J. Lyyränen, and J. Jokiniemi, "A novel field measurement method for determining fine particle and gas emissions from residential wood combustion," *Atmospheric Environment* **41,** 8330–8344 (2007).

[101] T. Kaivosoja, P. Jalava, H. Lamberg, A. Virén, M. Tapanainen, T. Torvela, U. Tapper, O. Sippula, J. Tissari, R. Hillamo, M. Hirvonen, and J. Jokiniemi, "Comparison of emissions and toxicological properties of fine particles from wood and oil boilers in small (20–25 kW) and medium (5–10 MW) scale," *Atmospheric Environment* **77** (2013).

[102] J. Leskinen, J. Tissari, O. Uski, A. Virén, T. Torvela, T. Kaivosoja, H. Lamberg, I. Nuutinen, T. Kettunen, J. Joutsensaari, P. Jalava, O. Sippula, M. Hirvonen, and J. Jokiniemi, "Fine particle emissions in three different combustion conditions of a wood chip-fired appliance – Particulate physico-chemical properties and induced cell death," *Atmospheric Environment* **86,** 129–139 (2014).

[103] M. Tapanainen, P. I. Jalava, J. Mäki-Paakkanen, P. Hakulinen, M. S. Happo, H. Lamberg, J. Ruusunen, J. Tissari, K. Nuutinen, P. Yli-Pirilä, R. Hillamo, R. O. Salonen, J. Jokiniemi, and M. Hirvonen, "In vitro immunotoxic and genotoxic activities of particles emitted from two different small-scale wood combustion appliances," *Atmospheric Environment* **45,** 7546–7554 (2011).

[104] H. Lamberg, K. Nuutinen, J. Tissari, J. Ruusunen, P. Yli-Pirilä, O. Sippula, M. Tapanainen, P. Jalava, U. Makkonen, K. Teinilä, K. Saarnio, R. Hillamo, M.-R. Hirvonen, and J. Jokiniemi, "Physicochemical characterization of fine particles from small-scale wood combustion," *Atmospheric Environment* **45,** 7635–7643 (2011).

[105] O. Hänninen, K. Koistinen, A. Kousa, J. Keski-Karhu, and M. Jantunen, "Quantitative analysis of environmental factors in differential weighing of blank Teflon filters," *Journal of the Air & Waste Management Association* (2002).

[106] National Institute for Occupational Safety and Health (NIOSH), ed., *NIOSH Elemental Carbon (Diesel particulate) Method 5040*, 4 ed. (NIOSH, Atlanta, GA, USA, 1999).

[107] R. W. Cheary and A. Coelho, "Fundamental parameters approach to X-ray line-profile fitting," *Journal of Applied Crystallography* **25,** 109–121 (1992).

[108] Y. Chen, N. Shah, F. E. Huggins, and G. P. Huffman, "Transmission electron microscopy investigation of ultrafine coal fly ash particles," *Environmental Science and Technology* **39,** 1144–1151 (2005).

[109] H. Wiinikka, R. Gebart, C. Boman, D. Boström, A. Nordin, and M. Öhman, "High-temperature aerosol formation in wood pellets flames: Spatially resolved measurements," *Combustion and Flame* **147** (2006).

[110] S. Enestam, K. Mäkelä, R. Backman, and M. Hupa, "Occurrence of zinc and lead in aerosols and deposits in the fluidized-bed combus-

tion of recovered waste wood. Part 2: Thermodynamic considerations," *Energy & Fuels* **25,** 1970–1977 (2011).

[111] O. Uski, P. Jalava, M. Happo, J. Leskinen, O. Sippula, J. Tissari, J. Mäki-Paakkanen, J. Jokiniemi, and M.-R. Hirvonen, "Different toxic mechanisms are activated by emission PM depending on combustion efficiency," *Atmospheric Environment* **89,** 623–632 (2014).

[112] P. I. Jalava, M. S. Happo, J. Kelz, T. Brunner, P. Hakulinen, J. Mäki-Paakkanen, A. Hukkanen, J. Jokiniemi, I. Obernberger, and M. Hirvonen, "In vitro toxicological characterization of particulate emissions from residential biomass heating systems based on old and new technologies," *Atmospheric Environment* **50,** 24–35 (2012).

[113] Y. Chen, N. Shah, A. Braun, F. E. Huggins, and G. P. Huffman, "Electron Microscopy Investigation of Carbonaceous Particulate Matter Generated by Combustion of Fossil Fuels," *Energy & Fuels* **19,** 1644–1651 (2005).

[114] P. J. Harris, "Fullerene-like models for microporous carbon: a review," *Journal of Materials Science* **48,** 565–577 (2013).

[115] J. Tissari, J. Lyyränen, K. Hytönen, O. Sippula, U. Tapper, A. Frey, K. Saarnio, A. Pennanen, R. Hillamo, R. Salonen, M.-R. Hirvonen, and J. Jokiniemi, "Fine particle and gaseous emissions from normal and smouldering wood combustion fired in a conventional masonry heater," *Atmospheric Environment* **42,** 7862–7873 (2008).

[116] R. Egerton, R. McLeod, F. Wang, and M. Malac, "Basic questions related to electron-induced sputtering in the TEM," *Ultramicroscopy* **110,** 991–997 (2010).

[117] R. B. Reed, D. A. Ladner, C. P. Higgins, P. Westerhoff, and J. F. Ranville, "Solubility of nano-zinc oxide in environmentally and biologically important matrices," *Environmental toxicology and chemistry* **31,** 93–99 (2012).

[118] Y. Yin, Q. Lin, H. Sun, D. Chen, Q. Wu, X. Chen, and S. Li, "Cytotoxic effects of ZnO hierarchical architectures on RSC96 Schwann cells," *Nanoscale Research Letters* **7** (2012), ID:439.

[119] P. Jalava, R. Salonen, K. Nuutinen, A. Pennanen, M. Happo, J. Tissari, A. Frey, R. Hillamo, J. Jokiniemi, and M.-R. Hirvonen, "Effect of combustion condition on cytotoxic and inflammatory activity of residential wood combustion particles," *Atmospheric Environment* **44,** 1691–1698 (2010).

[120] I. Hsiao and Y. Huang, "Effects of various physicochemical characteristics on the toxicities of ZnO and TiO nanoparticles toward human lung epithelial cells.," *The Science of the total environment* **409,** 1219–1228 (2011).

[121] C. Shen, S. A. James, M. D. de Jonge, T. W. Turney, P. F. A. Wright, and B. N. Feltis, "Relating Cytotoxicity, Zinc Ions, and Reactive Oxygen in ZnO Nanoparticle–Exposed Human Immune Cells," *Toxicological Sciences* **136,** 120–130 (2013).